DISCLAIMER

This report was prepared as an account of work sponsored by an agency of the United States Government. Neither the United States Government nor any agency thereof, nor any of their employees, makes any warranty, express or implied, or assumes any legal liability or responsibility for the accuracy, completeness, or usefulness of any information, apparatus, product, or process disclosed, or represents that its use would not infringe privately owned rights. Reference herein to any specific commercial product, process, or service by trade name, trademark, manufacturer, or otherwise does not necessarily constitute or imply its endorsement, recommendation, or favoring by the United States Government or any agency thereof. The views and opinions of authors expressed herein do not necessarily state or reflect those of the United States Government or any agency thereof. Reference herein to any social initiative (including but not limited to Diversity, Equity, and Inclusion (DEI); Community Benefits Plans (CBP); Justice 40; etc.) is made by the Author independent of any current requirement by the United States Government and does not constitute or imply endorsement, recommendation, or support by the United States Government or any agency thereof.

INL/JOU-25-88349-Rev000

Comparison of Nuclear Thermal Propulsion Reactor Cores Using Different Fuel Forms, Neutron Spectra, and Uranium Enrichments

October 2025

Author: G. J. Youinou

Changing the World's Energy Future

Idaho National Laboratory

INL is a U.S. Department of Energy National Laboratory operated by Battelle Energy Alliance, LLC

INL/JOU-25-88349-Rev000

Comparison of Nuclear Thermal Propulsion Reactor Cores Using Different Fuel Forms, Neutron Spectra, and Uranium Enrichments

G. J. Youinou

October 2025

Idaho National Laboratory
Nuclear Science & Technology Directorate
Nuclear Reactor Technology Division
Idaho Falls, Idaho 83415

http://www.inl.gov

Prepared for the
U.S. Department of Energy
Office of Nuclear Energy
Under DOE Idaho Operations Office
Contract DE-AC07-05ID14517

Page intentionally left blank

Comparison of Nuclear Thermal Propulsion Reactor Cores Using Different Fuel Forms, Neutron Spectra, and Uranium Enrichments

G. J. Youinou, Idaho National Laboratory

Abstract. *A comparison of 300 MW HEU and HALEU NTP cores using different fuel forms is presented to demonstrate trends and potentially inform fuel development. Compared to HEU, HALEU cores require additional in-core moderation. Beryllium was chosen as the reference in-core moderator material; metal hydrides may also be considered. Typical NTP fuel forms such as carbide solid solutions, carbide-graphite composites, CERMETs and CERCERs were considered together with less typical fuel forms such as UC and U metal. The core and reflector masses add up to 1.9-2.7 and 0.9-2.0 metric tons for HALEU and HEU configurations, respectively. HALEU loading is very sensitive to the amount of in-core moderation which may impose tight fabrication tolerances. HALEU cores require more reactivity control mechanisms than some HEU cores to compensate for temperature feedback and to ensure they remain subcritical in case of water ingress. Using enrichments slightly above HALEU (e.g., 25%) may provide a compromise between the administrative preference for using HALEU and the engineering preference for simplifying the reactor systems by, for example, not using in-core moderators.*

1. Introduction and Objective

Several nuclear fuel forms have been proposed for Nuclear Thermal Propulsion (NTP) cores, and only a few recent comparisons of the impact on core design appear to be available (e.g., [Nelson, 2020], [Poston, 2018], [Fittje, 2015]). The objective of this report is to contribute to such comparisons by evaluating critical fuel loadings, reactor masses, and the effects of temperature and water ingress on reactivity for different fuel forms and considering fast, intermediate and thermal neutron spectrum cores using either HEU or HALEU.

To enable systematic comparisons, independent of the fuel form, all cores generate the same thermal power (300 MW) and have the same number of fuel assemblies, same fuel assembly outer dimensions, same hydrogen flow surface area, and same inlet/outlet temperatures. These comparisons are meant to demonstrate trends to inform potential fuel development and should not be understood as comparisons between optimized fuel/core configurations.

2. Fuel Forms and Densities

The following typical NTP fuel forms were considered: (**1**) (U,Zr)C carbide solid solutions, (**2**) (U,Zr)C-graphite composite (historical NERVA fuel), (**3**) (U,Zr,X)C carbide solid solutions with X = Nb and Ta, (**4**) UN/W CERMET (coated UN fuel particles in a W matrix), (**5**) UN/Mo CERMET (coated UN fuel particles in a Mo matrix), (**6**) UN/ZrC CERCER (coated UN fuel particles in a ZrC matrix), (**7**) (U,Zr)CN carbonitride solid solution. In addition, two less typical fuel forms for NTP applications were also considered: (**8**) uranium carbide (UC), (**9**) uranium metal (U).

To compare different fuel forms, it is necessary to have a reasonably consistent set of densities. This section presents the fuel component densities estimated with the rule of mixtures for the solid solutions (carbides and carbonitrides), and with volume weighting for the CERMET and CERCER. Typical fuel design variables are considered, i.e., mole fractions in solid solutions, volume fractions in composites (CERMET, CERCER), and a combination of both for the "NERVA". Impurities were not considered.

2.1 (U,Zr)C carbide solid solutions

$(U_x,Zr_{1-x})C$ carbide solid solutions were tested during the Rover/NERVA program but only with a relatively small U loading of 0.31-0.32 g/cm^3 corresponding to x ~ 0.025 (see Table VI in [Lyon, 1973]). More recently, $(U_x,Zr_{1-x})C$ carbides with x up to 0.3 have been synthetized and characterized (see, for example, [Kardoulaki, 2022], [Schaeperkoetter, 2025], [Kardoulaki, 2025]). Table 2-1 shows a reasonable agreement

between theoretical densities calculated from crystal structure [Schaeperkoetter, 2025] and those estimated from the rule of mixtures (see details in Appendix A).

Table 2-1. Calculated $(U_x,Zr_{1-x})C$ theoretical densities for x = 0.05-0.3.

U mole fraction x	0.05	0.1	0.2	0.3
Crystal structure [Schaeperkoetter, 2025]	7.05	7.46	8.19	8.97
Rule of mixtures (this work)	7.14	7.54	8.31	9.06
Difference	1.3%	1.1%	1.5%	1.0%

Fig. 2-1 shows the estimated U, Zr, and C densities in $(U_x,Zr_{1-x})C$ carbide solid solutions as a function of the U mole fraction, x, and assuming 10% porosity.

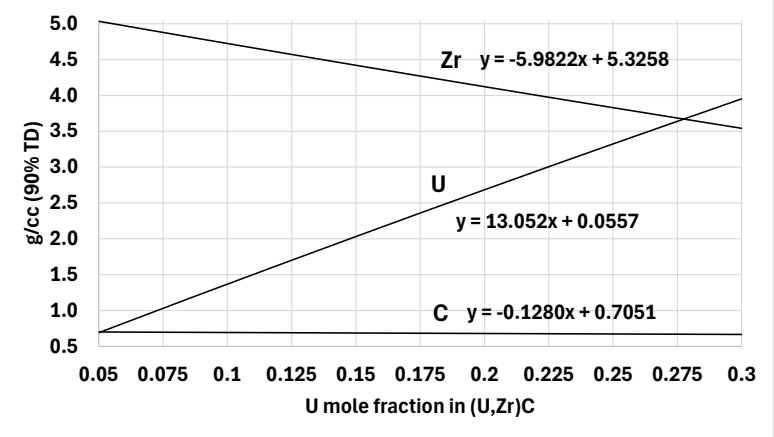

Fig. 2-1.
Estimated U, Zr, and C densities in $(U_x,Zr_{1-x})C$ solid solution as a function of U mole fraction x.

It is noteworthy that the $(U_x,Zr_{1-x})C$ solidus temperature decreases as x increases (Fig. 2-2) and, consequently, small U loadings are preferable. Thermal conductivity is shown in Fig. 2-3; a conservative value of 0.2 W/cmK was considered for peak temperature evaluations (Section 9).

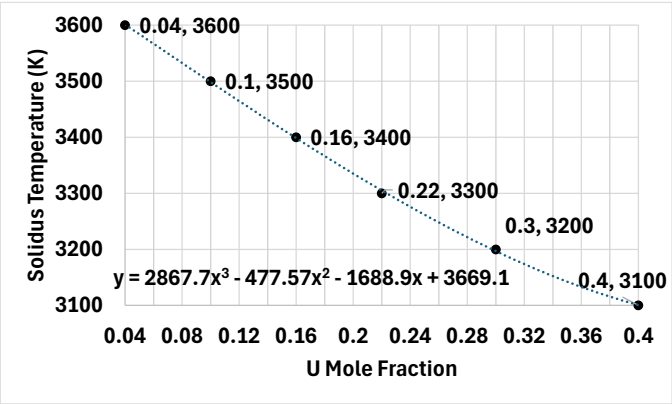

Fig. 2-2.
Estimated $(U_x,Zr_{1-x})C_{0.81}$ solidus temperature as a function of the U mole fraction x.
Adapted from Fig. 4 in [Butt, 1993].

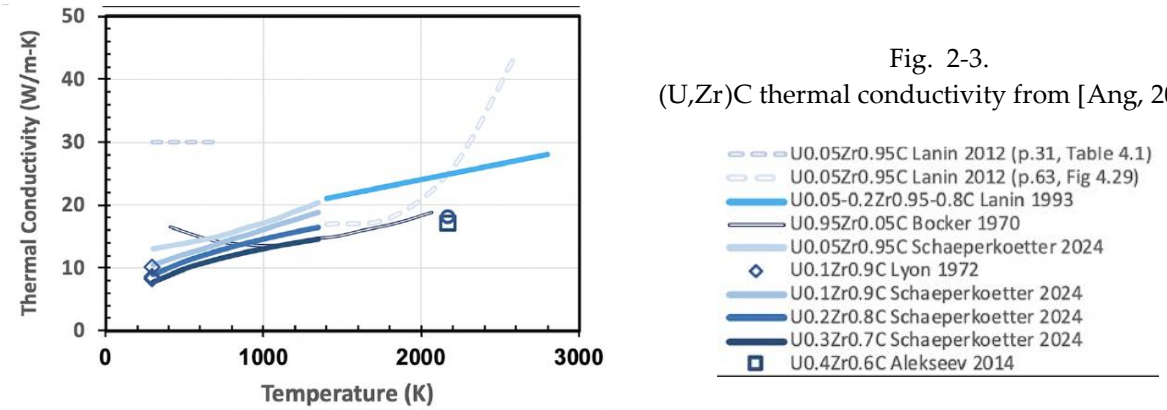

Fig. 2-3.
(U,Zr)C thermal conductivity from [Ang, 2025].

2.2 (U,Zr)C-graphite composite (historical NERVA fuel)

This fuel is made up of uncoated (U_x,Zr_{1-x})C carbide solid solution particles dispersed in a graphite matrix. It was tested during the Rover/NERVA program with up to 45 vol% carbide and U loadings up to 0.65 g/cm^3 [Lyon, 1973]. The reference fuel contained 35 vol% carbide.

Fig. 2-4 shows the estimated U, Zr, C and graphite densities in these composites as a function of the U mole fraction and assuming 35 vol% carbide (the graphite matrix occupies the other 65 vol%) and 10% porosity. Using the data in this figure, the 0.65 g/cm^3 loading mentioned above corresponds to x = 13.8 mole%, which is consistent with the as-build data discussed in [Lyon, 1973]. A graphite feedstock density of 1.89 g/cm^3 was considered.

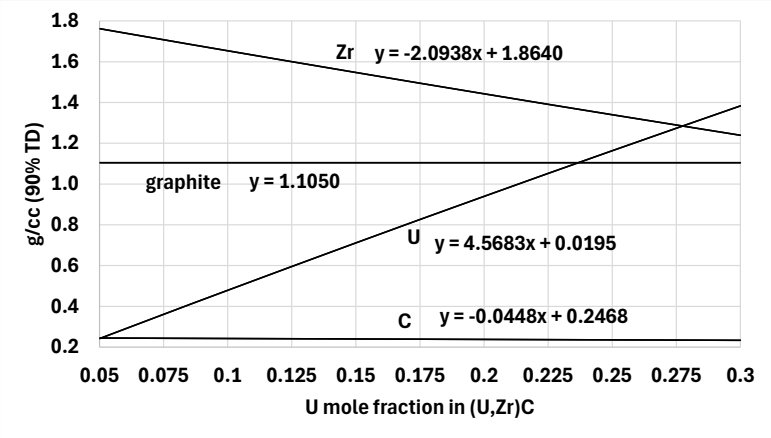

Fig. 2-4.
Estimated U, Zr, C and graphite densities in 35 vol% (U_x,Zr_{1-x})C and 65 vol% graphite composites as a function of U mole fraction x.

Graphite thermal conductivity decreases with temperature, and a conservative value of 0.2 W/cmK (see, for example, [Pavlov, 2020]) was considered for the peak temperature evaluations (Section 9). Under this conservative assumption, the thermal conductivity is the same for the (U,Zr)C/G composite and the (U,Zr)C solid solution, i.e. 0.2 W/cmK.

2.3 (U,Zr,X)C carbide solid solutions

(U,Zr,Nb)C was tested during the Russian space program in the form of twisted ribbons [Bhattacharyya, 2001]. Fig. 2-5 shows the estimated U, Zr, Nb and C densities in (U_x,Zr_y,Nb_y)C carbide solid solutions (with y = 0.5[1-x]) as a function of the U mole fraction and assuming 10% porosity. Solidus curves for the ZrC-NbC-UC system (see, for example, [Knight, 1999]) indicate that, for the same U loading, the melting temperatures of (U,Zr,Nb)C and (U,Zr)C are similar.

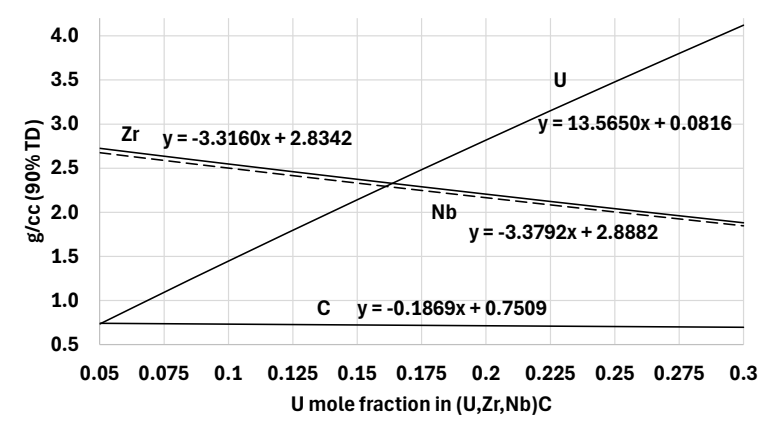

Fig. 2-5.
Estimated U, Zr, Nb, and C densities in (U_x,Zr_y,Nb_y)C solid solution (y = 0.5[1-x]) as a function of U mole fraction x.

(U,Zr,Ta)C was also investigated because of its potential for reaching higher temperatures than (U,Zr)C and (U,Zr,Nb)C [Bhattacharyya, 2001] [Knight, 1999]. The melting temperature of TaC is about 350 K higher than those of ZrC and NbC, so it seems reasonable to assume that the (U,Zr,Ta)C melting temperature is

also higher than those of (U,Zr)C and (U,Zr,Nb)C. However, (U,Zr,Ta)C phase diagrams are not readily available in the open literature. Fig. 2-6 shows the estimated U, Zr, Ta and C densities in $(U_x,Zr_y,Ta_y)C$ carbide solid solutions (with y = 0.5[1-x]) as a function of the U mole fraction and assuming 10% porosity. The details of the (U,Zr,Nb)C and (U,Zr,Ta)C theoretical density calculations are presented in Appendix A.

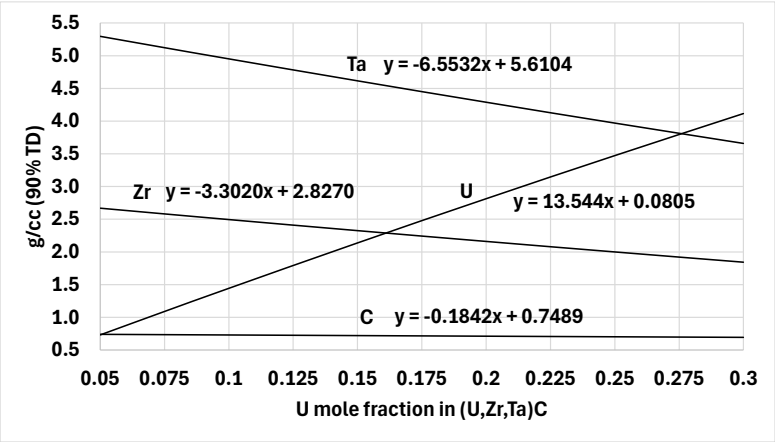

Fig. 2-6.
Estimated U, Zr, Ta, and densities in $(U_x,Zr_y,Ta_y)C$ solid solution (y = 0.5[1-x]) as a function of U mole fraction x.

2.4 UN/W CERMET

This fuel consists of W-coated UN particles embedded in a W matrix (T_{melt} = 3695 K) [Tucker, 2019] [Cröll, 2025]. The UN feedstock density is 13.59 g/cc, corresponding to 95% of its theoretical densities. The W matrix feedstock density is 19.25 g/cc. The CERMET has an assumed 5% porosity. The resulting UN and W densities in the CERMET are shown in Fig. 2-7. UN and W thermal conductivities are shown in Fig. 2-8 and the resulting CERMET thermal conductivities, estimated with the rule of mixtures (i.e., $1/k_{CERMET} = V_{UN}/k_{UN} + (1-V_{UN})/k_W$, where V_{UN} is the UN volume fraction in the CERMET), are shown in Fig. 2-9.

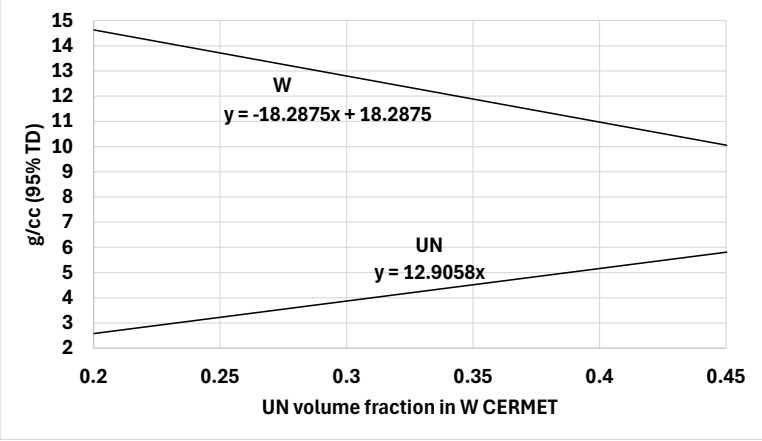

Fig. 2-7.
Estimated UN and W densities in CERMET as a function of UN volume fraction.

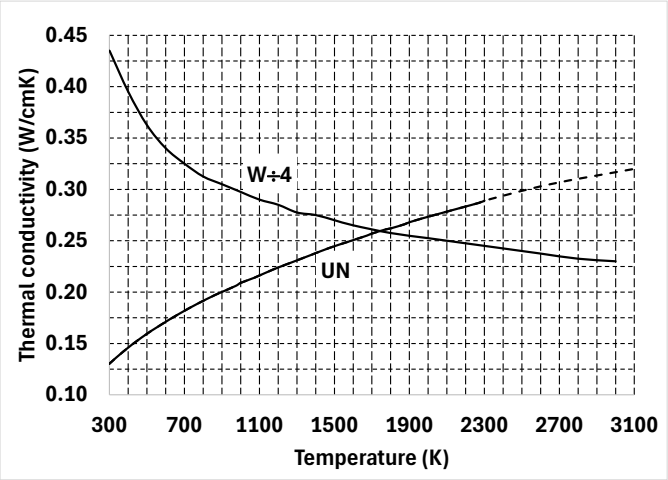

Fig. 2-8.
W and UN thermal conductivities.
[Bobkov, 2008] [Hust, 1984]

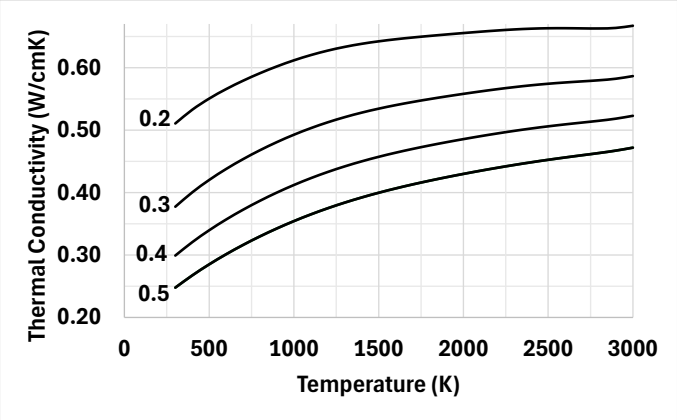

Fig. 2-9.
UN/W CERMET thermal conductivity estimated with the rule of mixtures as a function of temperature and for UN volume fractions of 0.2-0.5.

2.5 UN/Mo CERMET

This fuel consists of Mo-coated UN particles embedded in a Mo matrix (T_{melt} = 2895 K) [Tucker, 2019] [Raftery, 2021]. UN feedstock density is 13.59 g/cc corresponding to 95% of its theoretical densities. The Mo matrix feedstock density is 10.2 g/cc. The CERMET has an assumed 5% porosity. The resulting UN and Mo densities in the CERMET are shown in Fig. 2-10. The Mo and W thermal conductivities are similar and, consequently, the UN/Mo CERMETs thermal conductivities are close to those of the UN/W CERMETs.

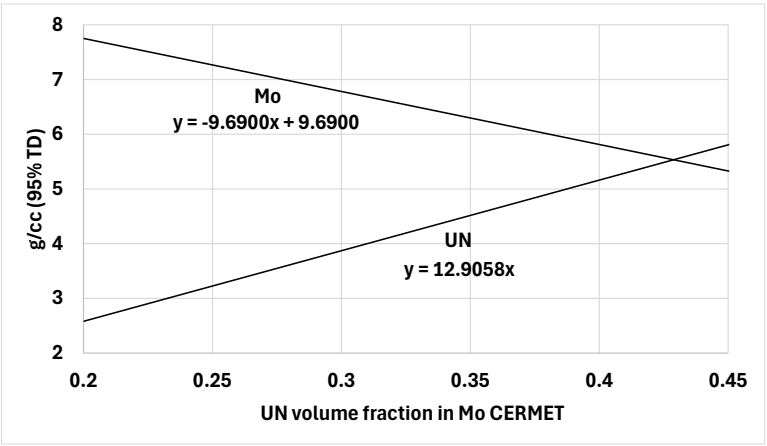

Fig. 2-10.
Estimated UN and Mo densities in CERMET as a function of UN volume fraction.

2.6 UN/ZrC CERCER

This fuel consists of ZrC-coated UN particles embedded in a ZrC matrix (T_{melt} = 3700 K) [Palomares, 2023] [Gustafson, 2021]. The UN and ZrC feedstock densities are 13.59 and 6.39 g/cc corresponding to 95% of their theoretical density. The CERCER composite has an assumed 5% porosity. Fig. 2-11. shows the estimated UN, Zr and C densities as a function of the UN volume fraction.

There is significant spread in the literature regarding ZrC thermal conductivity data as a function of temperature (see, for example, Fig. 2-12). A conservative value of 0.3 W/cmK was considered for the peak temperature evaluations and the resulting UN/ZrC CERCER thermal conductivities obtained with the rule of mixtures are shown in Fig. 2-13.

2.7 (U,Zr)CN carbonitride solid solution

This fuel contains the same components as the UN/ZrC CERCER though the fabrication processes are different [Hamilton, 2024]. For the same U loading, both fuels are neutronically equivalent. Fig. 2-14 shows the estimated U, Zr, N and C densities in $(U_x,Zr_{1-x})CN$ carbonitride solid solutions as a function of the U mole fraction, x, and assuming 10% porosity (see details of the theoretical densities estimation in Appendix B).

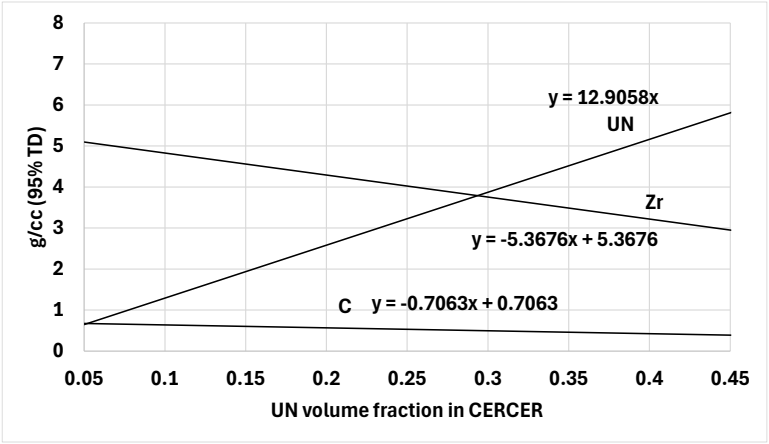

Fig. 2-11.
Estimated UN, Zr and C densities in CERCER as a function of UN volume fraction.

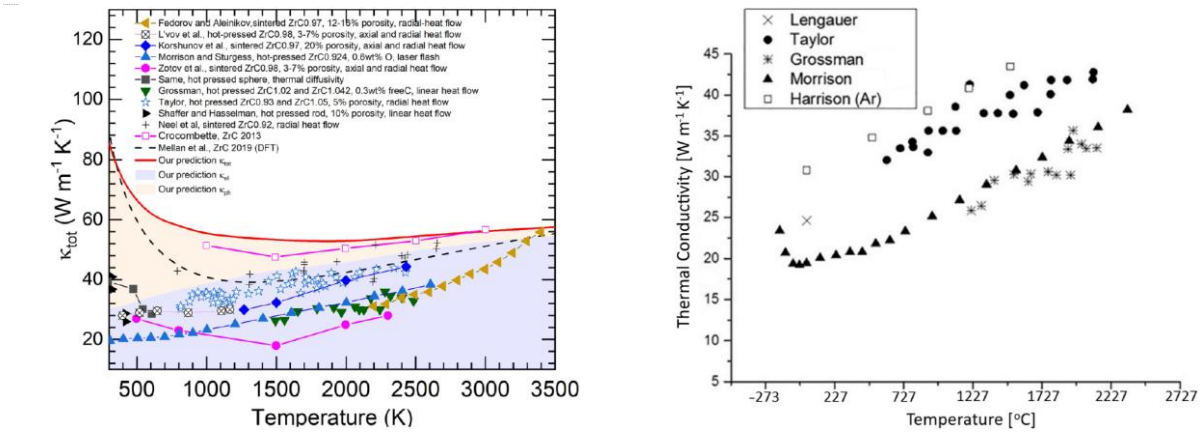

Fig. 2-12. Example of ZrC thermal conductivity data as a function of temperature from [Tiwari, 2023] (left) and [Peterson, 2023] (right).

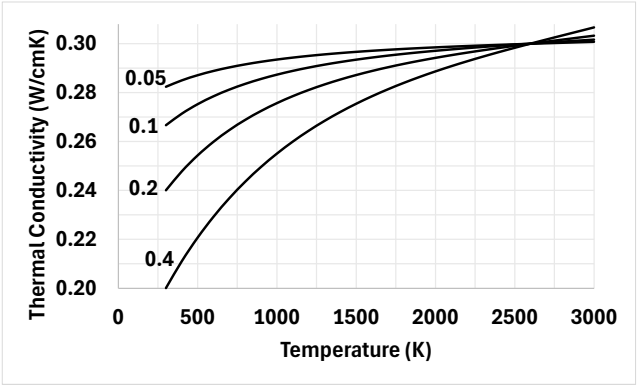

Fig. 2-13.
UN/ZrC CERCER thermal conductivity estimated with the rule of mixtures as a function of temperature and for UN volume fractions of 0.05-0.4.

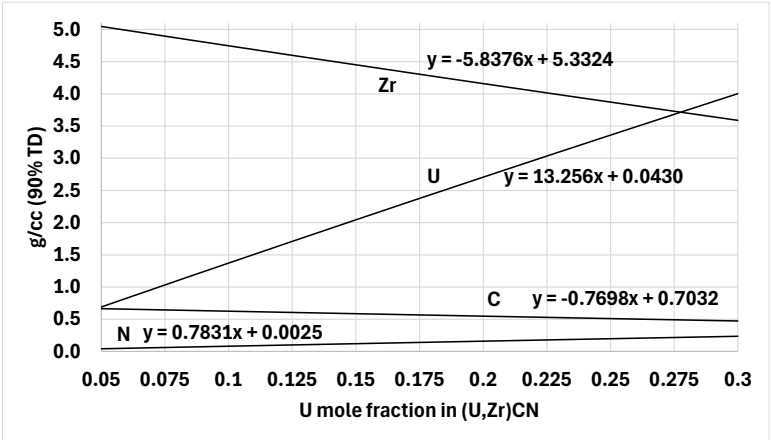

Fig. 2-14.
Estimated U, Zr, C and N densities in $(U_x,Zr_{1-x})CN$ solid solution as a function of U mole fraction x.

2.8 Monolithic UC

The UC density is 12.95 g/cc corresponding to 95% of its theoretical density. [Vasudevamurthy, 2022] recommends a melting temperature value of 2780 K. Thermal conductivity is shown in Fig. 2-15.

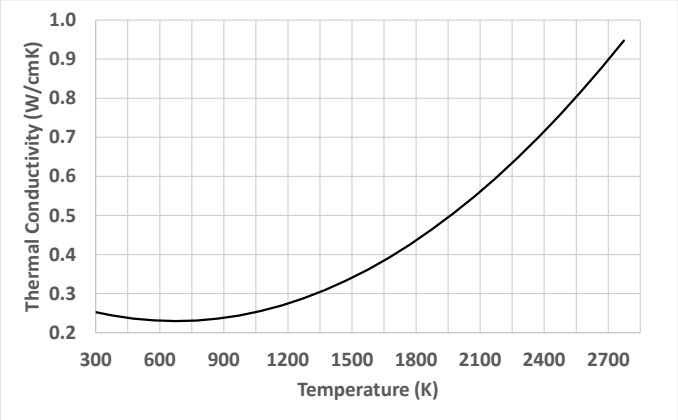

Fig. 2-15.
UC thermal conductivity as a function of temperature [Bobkov, 2008].

2.9 U Metal

U metal melts at 1405 K and boils at 4000-4400 K. The U (liquid) metal density assumed for the analyses is 16.26 g/cc, which corresponds to an average temperature of 1900 K [Bobkov, 2008]. The thermal conductivity of liquid uranium metal is lower than those of solid uranium metal or UC. A thermal conductivity value of 0.137 W/cmK was considered for the peak temperature evaluations, which corresponds to that at 1405 K [Bobkov, 2008].

2.10 Coated particle size considerations

It is useful to introduce a few parameters to discuss high-power density composite NTP nuclear fuels consisting of coated fuel particles dispersed in an inert matrix material.

The particle packing fraction (PPF) is the volume occupied by the particles per unit volume of composite (i.e., per unit volume of matrix + particles). The fuel kernel volume fraction within the particle (KVF_{part}) is obtained by dividing the volume of the fuel kernel by the volume of the particle. For spherical particles, $KVF_{part} = [1 \div (1+t_c/r_k)]^3$, where r_k is the fuel kernel radius and t_c is the coating thickness. The fuel kernel volume fraction within the composite (KVF_{comp}) is what characterizes the overall fuel phase loading in the composite. It can be expressed as:

$KVF_{comp} = PPF \times KVF_{part} = PPF \times [1 \div (1+t_c/r_k)]^3$

Furthermore, for a given core power, the power density inside the fuel kernel (W/cm^3), q_k, is proportional to the fuel phase volume, i.e., $q_k \propto KVF_{comp}$. This means that, for a given core power and PPF, many particle designs characterized by different t_c/r_k ratios yield the same q_k. For example, CERMET or CERCER fuels made up of 100-micron diameter fuel kernels surrounded by 5-micron coating or 200-micron diameter fuel kernels surrounded by 10-micron coating are characterized the same q_k.

Another important fuel performance parameter is the temperature gradient inside the fuel kernels:

$\Delta T_k = [q_k r_k^2] \div [6\lambda_k]$, where λ_k is the fuel kernel thermal conductivity (W/cmK).

Consequently, ΔT_k is proportional to $KVF_{comp} \times r_k^2$. As mentioned above, CERMET or CERCER fuel made up of 100-micron diameter fuel kernels surrounded by 5-micron coating or 200-micron diameter fuel kernels surrounded by 10-micron coating are characterized the same q_k. However, assuming a constant fuel kernel thermal conductivity, the temperature gradient in the 200-micron diameter fuel kernels will be 4 times larger than that in the 100-micron diameter fuel kernels.

3. Fuel Assembly Geometries

The typical block-type NTP fuel assembly (FA) geometry of the (U,Zr)C/Graphite composite and CERMET fuels is illustrated on Fig. 3-1. A 50-micron ZrC coating (T_{melt} = 3700 K) is applied on the (U,Zr)C/Graphite composite FA-1 surfaces to protect the graphite from reaction with H_2 [Fittje, 2015]. The CERMETs (FA-2) use a 200-micron W25Re cladding (T_{melt} = 3500 K) to minimize fuel loss at high temperature [Fittje, 2015].

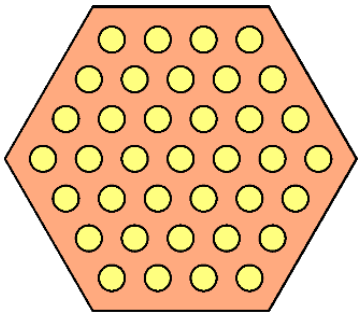

FA-1 & FA-2

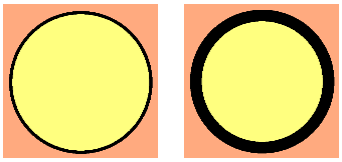

FA-1 channel **FA-2** channel

Closeup of FA-1 and FA-2 coolant channels showing the 50-micron ZrC coating (FA-1) and the 200-micron W25Re cladding (FA-2).

Fig. 3-1.
Illustration of (U,Zr)C/Graphite composite and CERMET FAs (FA-1 and FA-2, respectively) radial cross sections showing fuel (orange), cladding/coating (black), and coolant (yellow).

The FA-3 considered for the carbide solid solutions and CERCER are illustrated in Fig. 3-2. Though not exempt from H_2 reactions [Pelaccio, 1994], carbides are typically considered resistant enough that neither coating nor cladding are considered for the reference carbide FA-3s. That being said, (U,Zr)C was also considered with the same W25Re cladding as the CERMETs (FA-2) to quantify the effect. Dimensions are shown in Table 3-1.

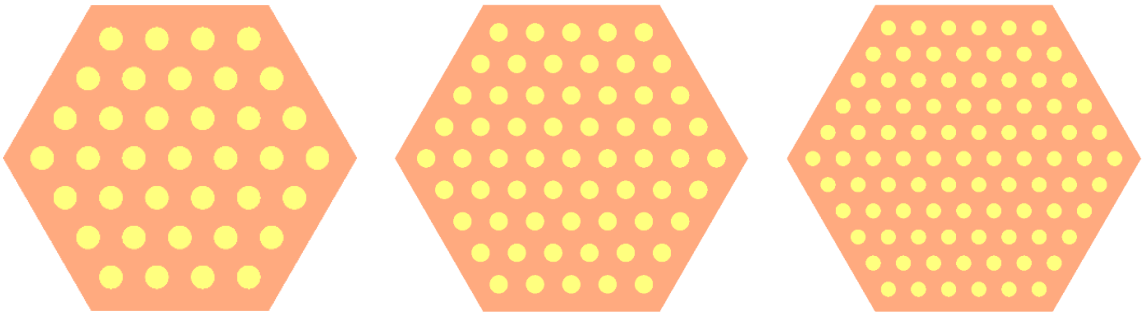

FA-3a (37 channels) **FA-3b** (61 channels) **FA-3c** (91 channels)

Fig. 3-2. Illustration of solid solutions and CERCER FAs radial cross sections (no cladding/coating) showing fuel (orange) and coolant channels (yellow).

As shown in Fig. 3-2, 37 to 91 coolant channels are considered for the solid solutions and CERCER FAs. As the number of coolant channels increases, both the diameter of the channels and the web thickness (Fig. 3-3) decrease (see Table 3-1). Trade-offs should be considered regarding these two important fuel design parameters. For example, a thin web is desirable to minimize fuel temperature, but it is undesirable from a structural strength point of view.

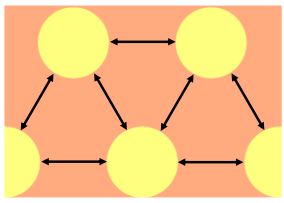

Fig. 3-3.
Illustration of the web thickness defined as the minimum distance between two coolant channels.

Less typical pin-type NTP FAs that use either UC or U metal were also considered as an alternative to the block types FAs. The fuel pins are assembled into tight triangular arrays and use a W25Re cladding. For this fuel type, the main challenge would likely be to properly seal the W25Re tubes at the outlet side. The advantage of using liquid U is that it ensures there is no gap between the fuel and the cladding that could potentially yield large temperature gradients.

Table 3-1. Carbide-graphite composite, CERMET, single phase carbides and CERCER FA dimensions.

	FA-1	FA-2	FA-3a	FA-3b	FA-3c
Fuel type	(U,Zr)C/G composite	CERMET	Carbide[a] CERCER	Carbide[a] CERCER	Carbide[a] CERCER
Active height (cm)	80	80	80	80	80
FA outer flat-to-flat (cm)	2.682	2.682	2.682	2.682	2.682
Coating/cladding thickness (microns)	50 (ZrC)	200 (W25Re)	N/A	N/A	N/A
Fuel flat-to-flat (cm)	2.672	2.642	2.682	2.682	2.682
# Coolant channels	37	37	37	61	91
Coolant channel inner diameter (cm)	0.207	0.207	0.207	0.161	0.132
Coating/cladding thickness (microns)	50 (ZrC)	200 (W25Re)	N/A	N/A	N/A
Coolant channel outer diameter (cm)	0.217	0.247	0.207	0.161	0.132
Fuel web thickness (cm)	0.244	0.209	0.256	0.199	0.163
Coolant flow surface area (cm^2)	1.246	1.246	1.246	1.246	1.246
Heat transfer surface area (cm^2)	1925	1925	1925	2472	3019
Fuel assembly volume (cm^3)	498.3	498.3	498.3	498.3	498.3
Fuel volume (cm^3)	385.1	341.7	398.6	398.6	398.6
Hydraulic diameter (cm)	0.207	0.207	0.207	0.161	0.132
S/V (cm^{-1})	3.86	3.86	3.86	4.96	6.06
Volume fractions					
Fuel	0.7728	0.6857	0.8000	0.8000	0.8000
Coolant	0.2000	0.2000	0.2000	0.2000	0.2000
Coating/cladding	0.0272	0.1143	0.0000	0.0000	0.0000

[a] (U,Zr)C ; (U,Zr,Nb)C ; (U,Zr,Ta)C ; (U,Zr)CN

Fig. 3-4 illustrates externally cooled annular fuel pins with a central graphite rodlet (FA-4) and an internally cooled pin FA concept in which the pins are positioned inside a graphite block (FA-5). Dimensions are shown in Tables 3-2 and 3-3. As illustrated in Fig. 3-4 (right), the FA-5 internally cooled pins have fins to increase the heat transfer surface area. The FA-4 and FA-5 have slightly different pin dimensions depending on whether they use UC or U metal; hence both FAs have a UC version and a U version.

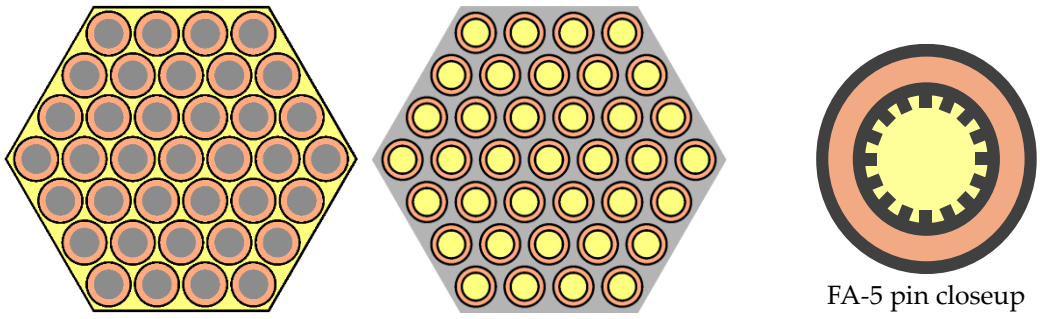

FA-4 **FA-5**

Fig. 3-4.Illustration of externally and internally cooled pin-type FAs (FA-4 and FA-5, respectively) showing fuel (orange), coolant (yellow), cladding (black), and graphite structure (gray).

It is noteworthy that the FAs using U metal have a thicker cladding (373 microns for FA-5/U and 400 microns for FA-4/U) than those using UC (200 microns) because liquid U penetrates W containers to some extent. For example, [Kuznietz, 1988] measured a 15-micron penetration of 1483 K liquid U in a 300-micron W foil after 2.5 hours. Following experimental investigations, [Das, 1981] concluded that W may be suitable to contain liquid U up to 2500 K for several hours. If necessary, the FA-4/U and FA-5/U could accommodate thicker W25Re cladding.

Table 3-2. Externally cooled annular pin FA dimensions.

	FA-4/UC	FA-4/U
Fuel type	UC	U
Active height (cm)	80	80
W25Re duct outer/inner flat-to-flat (cm)	2.682/2.642	2.682/2.642
# pins	37	37
W25Re cladding outer/inner diameter (cm)	0.406/0.366	0.406/0.326
W25Re cladding thickness (microns)	200	400
Fuel outer/inner diameter (cm)	0.366/0.316	0.326/0.273
Fuel thickness (microns)	250	265
Graphite rodlet diameter (cm)	0.316	0.273
Coolant flow surface area (cm^2)	1.246	1.246
Heat transfer surface area (cm^2)	3779	3779
Hydraulic diameter (cm)	0.0884	0.0884
Fuel assembly volume (cm^3)	498.3	498.3
Fuel volume (cm^3)	79.73	74.50
S/V (cm^{-1})	7.58	7.58
Volume fractions		
Fuel	0.1600	0.1495
Coolant	0.2000	0.2000
W25Re cladding and duct	0.1738	0.3031
Central graphite rodlets inside pins	0.4661	0.3474

Table 3-3. Internally cooled pin-type fuel assembly dimensions

	FA-5/UC	FA-5/U
Fuel type	UC	U
Active height (cm)	80	80
Graphite block outer flat-to-flat (cm)	2.682	2.682
# pins	37	37
W25Re outer cladding outer/inner diameter (cm)	0.370/0.330	0.433/0.358
W25Re outer cladding thickness (microns)	200	375
Fuel outer/inner diameter (cm)	0.330/0.264	0.358/0.298
Fuel thickness (microns)	330	300
W25Re inner cladding outer/inner diameter (cm)	0.264/0.224	0.298/0.224
W25Re inner cladding thickness (microns)	200	375
W25Re fins length/width/pitch (microns)	200/200/500	200/200/500
Coolant flow surface area (cm^2)	1.246	1.246
Heat transfer surface area (cm^2)	3737	3737
Hydraulic diameter (cm)	0.107	0.107
Fuel assembly volume (cm^3)	498.3	498.3
Fuel volume (cm^3)	91.94	91.44
S/V (cm^{-1})	7.50	7.50
Volume fractions		
Fuel	0.1845	0.1835
Coolant	0.2000	0.2000
W25Re cladding and fins	0.2549	0.4905
Graphite block	0.3606	0.1260

4. Core Configurations

Independent of the fuel form and uranium enrichment, all cores generate 300 MW with 211 hexagonal FAs (2.68-cm flat-to-flat, 80-cm active height, uniform U loading) surrounded by a 20-cm beryllium (Be) radial reflector. Neither axial reflectors nor control drums are considered at this point (fuel loadings should decrease when an axial reflector is considered). As a first approximation, hydrogen inlet/outlet temperatures are 350/2700 K for all fuels even though not all of them may be able to reach this outlet temperature; the corresponding hydrogen mass flow is 7.7 kg/s. Such a core would generate about 15,000 lbf (66.7 kN) of thrust with a specific impulse of about 900 seconds. The average FA power density is the same in all cores and equal to 2.85 kW/cm^3 which corresponds to a peak FA power density of about 5 kW/cm^3. HEU and HALEU core configurations are illustrated in Fig. 4-1 and 4-2.

HEU cores all have the same core + reflector diameter and active height (83.4 cm and 80 cm, respectively). The HALEU core configurations require in-core neutron moderation as well as thermal insulation between the FAs and the moderator (Fig. 4-3). Beryllium is considered as the reference in-core moderator material. Coolant channels inside the moderator are necessary to ensure its temperature remains acceptable; these were not considered here. The presence of coolant channels results in a decrease in the effective moderator density and, consequently, a larger pitch would be necessary. Instead of Be, metal hydrides such as ZrH_x or YH_x could also be considered; these would in principle enable smaller FA pitches than with Be.

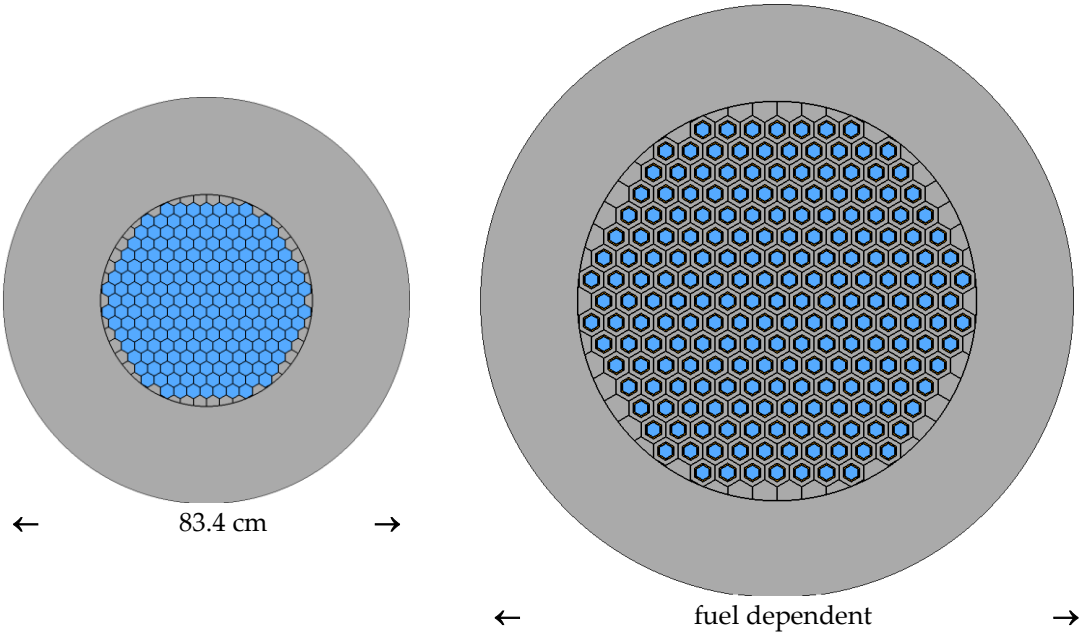

Figure 4-1. Radial cross section of HEU cores (left) and HALEU cores (right) showing the FA (blue) and the Be moderator/reflector (gray).

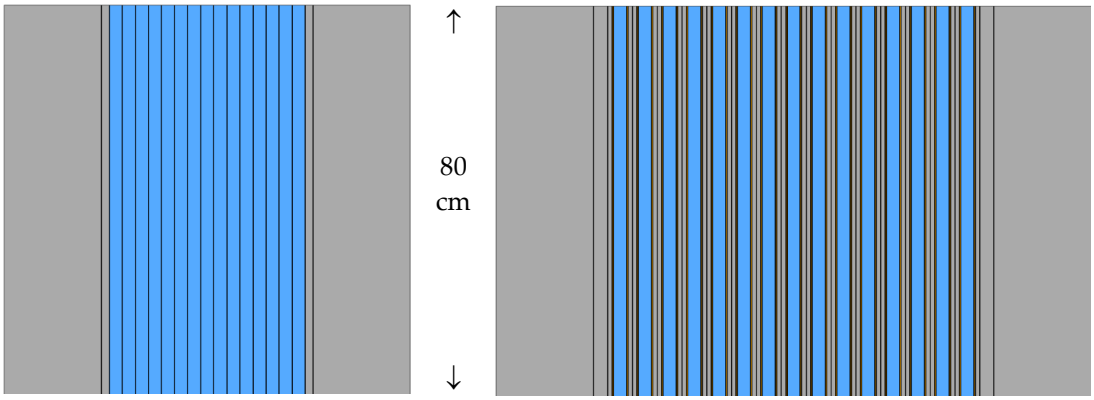

Figure 4-2. Axial cross section of HEU cores (left) and HALEU cores (right) showing the FA (blue) and the Be moderator/reflector (gray).

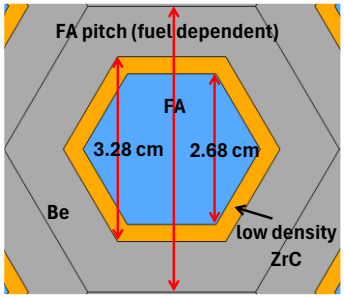

Figure 4-3.
Close-up of a HALEU core showing the FA (blue), the 3-mm-thick low-density ZrC thermal insulation (orange) and the Be in-core moderator block (gray).

It is noteworthy that, unlike metal hydrides that gradually lose their ability to moderate neutrons efficiently above their decomposition temperatures (~500-900 K in vacuum), Be retains its neutron moderation ability above its melting temperature (1560 K). Hence, compared to metal hydrides, Be can operate over a larger temperature range and, consequently, may be better able to recover from off-normal conditions. Even if a limited section of the Be moderator were to melt, it would not unduly impact reactor operation if it remained in place.

5. Critical Fuel Compositions and Core Bills of Materials

5.1 Methodology

The critical fuel compositions were estimated with the Monte-Carlo code KENO-VI and its associated continuous energy ENDF/B-VIII.0-based nuclear data library [Wieselquist, 2023]. The calculations are performed assuming fuel and Be temperatures of 2000 K and 900 K, respectively. The target k-eff-HOT is 1.02.

5.2 HEU cores

Since the HEU cores and FA dimensions are fixed, the only degree of freedom left to meet the required HEU critical mass is the fuel composition. For the (U,Zr)C/G composites, two parameters can in principle be adjusted, i.e., the carbide volume fraction in the composite and the U mole fraction in the carbide. For this analysis, the carbide volume fraction was fixed at 35%, corresponding to the reference NERVA fuel, and the U mole fraction in the carbide was adjusted. For the CERMET and CERCER, only one parameter can be adjusted, i.e. the UN volume fraction in the matrix. For the solid solutions, only one parameter can be adjusted, i.e. the U mole fraction. The critical fuel compositions obtained are summarized in Table 5-1.

The U loading in the (U,Zr)C/G composite (0.824 g/cm^3) is higher than what was tested during the Rover/NERVA program (0.65 g/cm^3). Past reactor analyses using this composite fuel (e.g., [Schnitzler, 2009], [Schnitzler, 2010], [Schnitzler, 2011], [Fittje, 2015]) do not exceed this value to remain within a range of tested fuel compositions. To do so, metal hydride moderator is typically used to increase neutron moderation and to decrease U loading below 0.65 g/cm^3.

The KVF_{comp} in the CERMET FA-2 is between 0.310 (UN/W) and 0.265 (UN/Mo). A KVF_{comp} of 0.310 could be accommodated, for example, by using 200-micron diameter UN kernels surrounded by a 10-micron W coating (i.e., $KVF_{particle}$ = 0.751) and a PPF of 0.413. With lower KVF_{comp}, more [kernel diameter – coating thickness – PPF] combinations are possible which may be helpful for the fuel designer to find an optimal solution among the various design and fabrication trade-offs. With a KVF_{comp} of only 0.084, the CERCER FA-3 may have even more potential practical [kernel diameter – coating thickness – PPF] combinations to find an optimal solution.

The FA-3 carbide solid solution HEU loadings are 7.1, 10.5, and 20.2 mole % for (U,Zr)C, (U,Zr,Nb)C, and (U,Zr,Ta)C, respectively (0.99-2.8 gHEU/cm^3). Using a 200-micron W25Re cladding requires increasing the FA-2 U loading in (U,Zr)C to 18.7 mole % (2.5 gHEU/cm^3) to compensate the additional neutron absorption of the cladding.

Table 5-1. HEU fuel critical compositions.

Fuel Form	FA identifier	FA pitch (cm)	HEU fuel critical compositions (k-eff-HOT = 1.02)
Composite (U,Zr)C/G	FA-1	2.68	35 vol% (U,Zr)C ; 17.6 mole% U → 0.824 gU/cm^3
CERMET UN/W	FA-2	2.68	KVF_{comp} = 0.310 → 3.78 gU/cm^3
CERMET UN/Mo	FA-2	2.68	KVF_{comp} = 0.265 → 3.23 gU/cm^3
CERCER UN/ZrC	FA-3a/b/c	2.68	KVF_{comp} = 0.084 → 1.02 gU/cm^3
Solid Solution (U,Zr)CN	FA-3a/b/c	2.68	7.4 mole% U → 1.02 gU/cm^3
Solid Solution (U,Zr)C	FA-3a/b/c	2.68	7.1 mole% U → 0.987 gU/cm^3
Solid Solution (U,Zr,Nb)C	FA-3a/b/c	2.68	10.5 mole% U → 1.51 gU/cm^3
Solid Solution (U,Zr,Ta)C	FA-3a/b/c	2.68	20.2 mole% U → 2.84 gU/cm^3
Solid Solution (U,Zr)C	FA-2	2.68	18.7 mole% U → 2.51 gU/cm^3
UC pins. External Cooling	FA-4/UC	2.68	UC → 12.9 gU/cm^3
U pins. External Cooling	FA-4/U	2.68	U → 16.3 gU/cm^3
UC pins. Internal Cooling	FA-5/UC	2.68	UC → 12.9 gU/cm^3
U pins. Internal Cooling	FA-5/U	2.68	U → 16.3 gU/cm^3

The resulting HEU core bills of materials (BOM) are summarized in Table 5-2. The smallest U^{235} critical mass is obtained with the (U,Zr)C/G composite (62.3 kg) and the largest with the U metal pins (292 kg). Assuming the reactor operates for a typical 0.1 equivalent-full-power-day, it produces 30 MWd of thermal power which corresponds to 0.03 kg of fission products produced, i.e., 0.01%-0.045% of the initial HEU. The smallest core BOM is obtained with the (U,Zr)C/G composite (930 kg) and the largest with the UN/W CERMET (2047 kg).

Table 5-2. 300 MW HEU core BOMs.

Fuel Form	FA identifier	U (kg)	U^{235} (kg)	FA (kg)	Be refl (kg)	total (kg)	core+refl ∅/H_{act} (cm)
Composite (U,Zr)C/G 35 vol% 17.6% mole U	FA-1	66.9	62.3	317	613	930	83.4/80.0
CERMET UN/W, KVF_{comp} = 0.310	FA-2	272	253	1434	613	2047	83.4/80.0
CERMET UN/Mo, KVF_{comp} = 0.265	FA-2	233	217	996	613	1609	83.4/80.0
CERCER UN/ZrC, KVF_{comp} = 0.084	FA-3a/b/c	86.1	80.1	559	613	1172	83.4/80.0
Solid Solution (U,Zr)CN 7.4% mole U	FA-3a/b/c	86.1	80.1	559	613	1172	83.4/80.0
Solid Solution (U,Zr)C 7.1% mole U	FA-3a/b/c	83.0	77.2	554	613	1167	83.4/80.0
Solid Solution (U,Zr,Nb)C 10.5% mole U	FA-3a/b/c	127	118	610	613	1223	83.4/80.0
Solid Solution (U,Zr,Ta)C 20.2% mole U	FA-3a/b/c	239	222	839	613	1452	83.4/80.0
Solid Solution (U,Zr)C 18.7% mole U	FA-2	181	169	769	613	1382	83.4/80.0
UC pins. External Cooling	FA-4/UC	207	193	660	613	1273	83.4/80.0
U pins. External Cooling	FA-4/U	256	238	944	613	1557	83.4/80.0
UC pins. Internal Cooling	FA-5/UC	239	222	843	613	1456	83.4/80.0
U pins. Internal Cooling	FA-5/U	314	292	1350	613	1963	83.4/80.0

5.3 HALEU cores

Five of the previous twelve fuel forms are compatible with the use of HALEU in Be-moderated cores: (U,Zr)C, (U,Zr)C/G composite, (U,Zr,Nb)C, CERCER and (U,Zr)CN. Two degrees of freedom are available to reach the required HALEU critical mass, i.e., the fuel compositions and the amount of Be moderator in the core. Note that analyses presented in [Youinou, 2024] indicate that pin type FAs such as FA-4 may also be compatible with HALEU if less-absorbing cladding materials such as W40Mo could be used instead of the W25Re considered here.

A few examples of critical fuel compositions are shown in Table 5-3. It is significant that the required HALEU loading is very sensitive to the FA pitch (i.e., to the amount of in-core Be). For example, by increasing the (U,Zr)C solid solution FA pitch from 5.10 cm to 5.16 cm, the required HALEU loading decreases from 0.987 g/cm^3 to 0.708 g/cm^3, i.e. by 28%. Such large sensitivities translate into tight fabrication tolerances. It may also require additional reactivity control mechanisms in case the core excess reactivity is larger than expected. These observations are consistent with those discussed in [Poston, 2025].

Table 5-3. Examples of Be-moderated HALEU fuel critical compositions and FA pitch.

Fuel Form	FA identifier	FA pitch (cm)	HALEU fuel critical compositions (k-eff-HOT = 1.02)
Composite (U,Zr)C/G	FA-1	4.98	35 vol% (U,Zr)C & 17.6 mol% U → 0.824 gU/cm^3
		5.14	35 vol% (U,Zr)C & 10.0 mol% U → 0.478 gU/cm^3
CERCER UN/ZrC	FA-3a/b/c	5.18	KVF_{comp} = 0.084 → 1.02 gU/cm^3
		5.34	KVF_{comp} = 0.050 → 0.607 gU/cm^3
Solid Solution (U,Zr)CN	FA-3a/b/c	5.18	7.4 mol% U → 1.02 gU/cm^3
		5.34	4.3 mol% U → 0.607 gU/cm^3
Solid Solution (U,Zr)C	FA-3a/b/c	5.10	7.1 mol% U → 0.987 gU/cm^3
		5.16	5.0 mol% U → 0.708 gU/cm^3
Solid Solution (U,Zr,Nb)C	FA-3a/b/c	5.84	10.5 mol% U → 1.51 gU/cm^3
		6.22	5.5 mol% U → 0.832 gU/cm^3

The resulting 300 MW HALEU cores BOM are summarized in Table 5-4. The U^{235} critical masses of the configurations considered are all small (7.7-25.1 kg). The smallest BOM is obtained with the (U,Zr)C/G composite (1854 kg) and the largest with the (U,Zr,Nb)C solid solution (2726 kg).

It is noteworthy that the five Be-moderated HALEU core BOMs are about twice as large as those of their HEU counterparts: 1854 vs 930 kg for the (U,Zr)C/G composite, 2187 vs 1172 kg for the CERCER and the (U,Zr)CN, 2153 vs 1167 kg for the (U,Zr)C, and 2562 vs 1223 kg for the (U,Zr,Nb)C. (As a reminder, these comparisons are meant to demonstrate trends and should not be understood as being comparisons between optimized fuel/core configurations.)

Table 5-4. Examples of 300 MW Be-moderated HALEU core BOMs.

Fuel Form		U (kg)	U^{235} (kg)	FA (kg)	ZrC[a] (kg)	Be core (kg)	Be refl (kg)	total (kg)	core+refl ∅/H_{act} (cm)
Composite (U,Zr)C/G	17.6 mole% U	66.9	13.2	317	140	379	1018	1854	121/80.0
35 vol% carbide, FA-1	10.0 mole% U	38.9	7.7	302	140	423	1054	1919	123/80.0
CERCER UN/ZrC,	KVF_{comp} = 0.084	86.1	17.0	559	140	434	1054	2187	124/80.0
FA-3a/b/c	KVF_{comp} = 0.050	51.2	10.1	540	140	480	1089	2249	127/80.0
Sol. Sol. (U,Zr)CN,	7.4 mole% U	86.1	17.0	559	140	434	1054	2187	124/80.0
FA-3a/b/c	4.3 mole% U	51.2	10.1	540	140	480	1089	2249	127/80.0
Sol. Sol. (U,Zr)C,	7.1 mole% U	83.0	16.4	554	140	412	1047	2153	123/80.0
FA-3a/b/c	5.0 mole% U	59.5	11.8	541	140	429	1059	2169	124/80.0
Sol. Sol. (U,Zr,Nb)C,	10.5 mole% U	127	25.1	610	140	631	1181	2562	135/80.0
FA-3a/b/c	5.5 mole% U	70.0	13.8	582	140	754	1250	2726	141/80.0

[a] 3-mm thick low density ZrC thermal insulation between FAs and Be moderator.

To illustrate the impact of the moderator material, Table 5-5 shows the (U,Zr,Nb)C (10.5 mol% U) core BOM obtained with the reference Be moderator and with $ZrH_{1.6}$ (a density of 5.33 g/cm^3 was considered corresponding to 95% of its theoretical density). Compared to Be, the use of $ZrH_{1.6}$ enables a smaller pitch and, consequently, smaller core BOM (1828 kg vs 2562 kg). As mentioned previously, coolant channels in the moderator are necessary but were not considered here; their presence would require increasing the FA

pitch and, consequently, the mass of the radial reflector would also increase. Hence, even with the $ZrH_{1.6}$, the HALEU core BOM is still at least 50% larger than that of the HEU core.

Table 5-5. (U,Zr,Nb)C 10.5 mol%U core BOMs obtained with the reference Be moderator and with $ZrH_{1.6}$.

Fuel Form	Moderator Material	FA pitch (cm)	U (kg)	U^{235} (kg)	FA (kg)	ZrC[a] (kg)	mod (kg)	Be refl (kg)	total (kg)	core+refl ∅/H_{act} (cm)
(U,Zr,Nb)C,	Be (ref)	5.84	127	25.1	610	140	631	1181	2562	135/80.0
10.5 mol% U	$ZrH_{1.6}$	3.78	127	25.1	610	140	275	803	1828	101/80.0

[a] 3-mm thick low density ZrC thermal insulation between FAs and moderator.

5.4 HALEU+ cores

In this section U enrichment of 25% is referred to as HALEU+ even though this denomination does not actually exist; from a regulatory standpoint it is HEU. Such HALEU+ configurations may provide a compromise between the administrative preference for using HALEU and the engineering preference for simplifying the reactor systems as much as possible by, for example, not using in-core moderators.

Out of the previous twelve fuel forms, four may be able to accommodate HALEU+ without requiring in-core Be moderation: the (U,Zr)C solid solution, the UN/ZrC CERCER, the (U,Zr)CN solid solution and the externally cooled UC pins if the central graphite rodlet is removed and replaced with UC. This variant of the pin-type FA-4/UC is called FA-4'/UC; it is illustrated in Fig. 5-1, and its dimensions are presented in Table 5-6.

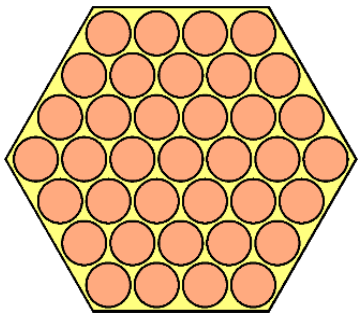

Fig. 5-1.

Radial cross sections of externally cooled **FA-4'/UC** showing fuel (orange), coolant (yellow), cladding (black).

Table 5-6. HALEU+ externally cooled cylindrical pin FA dimensions.

	FA-4'/UC
Fuel type	UC
Active height (cm)	80
W25Re duct outer/inner flat-to-flat (cm)	2.682/2.642
# pins	37
W25Re cladding outer/inner diameter (cm)	0.406/0.366
W25Re cladding thickness (microns)	200
Fuel outer diameter (cm)	0.366
Coolant flow surface area (cm^2)	1.246
Heat transfer surface area (cm^2)	3779
Hydraulic diameter (cm)	0.0884
Fuel assembly volume (cm^3)	498.3
Fuel volume (cm^3)	312.0
S/V (cm^{-1})	7.58
Volume fractions	
Fuel	0.6261
Coolant	0.2000
W25Re cladding and duct	0.1738

The HALEU+ critical compositions are shown in Table 5-7. The necessary HALEU+ loading in the (U,Zr)C is 39 mole% which may limit the outlet temperature compared to the other configurations (solidus temperature is 3100 K for 39 mole% U, whereas it is 3550 K for 7.1 mole% U). The UN volume fraction in the CERCER is higher than before (KVF_{comp} = 0.46). The HALEU+ loading in the (U,Zr)CN is 43 mole%.

As noted previously, these configurations are not optimized, and further analyses may yield lower U loadings. For example, consistently with the analyses presented in [Youinou, 2022], the FA-4'/UC U enrichment would decrease from 25% to 19.75% (i.e., HALEU) if W25Mo could be used instead of W25Re together with a slightly thicker radial reflector (22 cm instead of the reference 20 cm).

The resulting HALEU+ cores BOMs are summarized in Table 5-8. The smallest U^{235} critical mass is obtained with the CERCER (118 kg) and the largest with the UC pins (205 kg). The smallest core BOM is obtained with the (U,Zr)C (1348 kg) and the largest with the UC pin configuration (1825 kg).

Table 5-7. HALEU+ fuel critical compositions.

Fuel Form	FA identifier	FA pitch (cm)	HALEU+ fuel critical compositions (k-eff-HOT = 1.02)
Solid Solution (U,Zr)C	FA-3a/b/c	2.68	39 mol% U (25% U^{235}) → 5.05 gU/cm^3
CERCER UN/ZrC	FA-3a/b/c	2.68	KVF_{comp} = 46 vol% UN (25% U^{235}) → 5.61 gU/cm^3
Solid Solution (U,Zr)CN	FA-3a/b/c	2.68	43 mol% U (25% U^{235}) → 5.61 gU/cm^3
UC pins. External Cooling	FA-4'/UC	2.68	UC (25% U^{235}) → 12.9 gU/cm^3

Table 5-8. 300 MW HALEU+ core BOMs.

Fuel Form	FA identifier	U (kg)	U^{235} (kg)	FA (kg)	Be refl (kg)	total (kg)	core+refl ∅/H_{act} (cm)
Solid Solution (U,Zr)C, 39 mol% U	FA-3a/b/c	531	133	735	613	1348	83.4/80.0
CERCER UN/ZrC, 46 vol% UN	FA-3a/b/c	472	118	775	613	1388	83.4/80.0
Solid Solution (U,Zr)CN, 43 mol% U	FA-3a/b/c	472	118	775	613	1388	83.4/80.0
UC pins. External Cooling	FA-4'/UC	811	205	1212	613	1825	83.4/80.0

6. Neutron Fluxes

Peak neutron fluxes in a few selected FAs assuming radial and axial peaks of 1.2 and 1.4, respectively, are presented in Table 6-1. These steady-state peak neutron fluxes are higher than in any other existing reactors: 1.2-2.1·10^{16} n/cm^{2}s in the HEU cores and 0.8-1.2·10^{16} n/cm^{2}s in the HALEU cores.

Table 6-1. Peak FA neutron fluxes (radial peak = 1.2, axial peak = 1.4).

Fuel Form	Fuel Enrichment	Total Flux (n/cm^{2}s)	Flux > 0.1 MeV (n/cm^{2}s)	Flux < 1 eV (n/cm^{2}s)
(U,Zr)C/G, 17.6 mol% U	HEU	2.1·10^{16}	1.2·10^{16}	1.3·10^{14}
	HALEU	1.2·10^{16}	3.9·10^{15}	1.8·10^{15}
(U,Zr)C, 7.1 mol% U	HEU	2.0·10^{16}	1.3·10^{16}	1.4·10^{14}
	HALEU	1.1·10^{16}	3.8·10^{15}	1.4·10^{15}
(U,Zr,Nb)C, 10.5 mol% U	HEU	1.8·10^{16}	1.2·10^{16}	7.3·10^{13}
	HALEU	8.1·10^{15}	2.9·10^{15}	9.5·10^{14}
CERCER UN/ZrC, KVF_{comp} = 0.084	HEU	2.1·10^{16}	1.3·10^{16}	9.3·10^{13}
	HALEU	1.1·10^{16}	3.7·10^{15}	1.4·10^{15}
CERMET UN/W, KVF_{comp} = 0.310	HEU	1.3·10^{16}	1.0·10^{16}	1.3·10^{13}
UC pins. External Cooling	HEU	1.5·10^{16}	1.0·10^{16}	2.1·10^{13}
U pins. Internal Cooling	HEU	1.2·10^{16}	9.7·10^{15}	1.4·10^{13}

The HEU peak neutron fluxes above 0.1 MeV (~10^{16} n/cm^{2}s), a typical material damage indicator, are about 10-20 times higher than what can be achieved in existing high power material testing reactors such as ATR or HFIR (see, for example, [Youinou, 2017]). Hence, neutron damage accumulation rates in NTP fuel materials are very high and probably higher than what can realistically be tested on earth without a dedicated prototype. Neutron spectra are shown in Appendix C.

7. Effect of Temperatures on k-eff

The k-eff of NTP cores during normal operation can be impacted by movements of the reactivity control mechanisms and by variations in the temperatures of the components. As mentioned earlier, k-eff-HOT was obtained assuming that the fuel and the Be temperature are 2000 K and 900 K, respectively. An additional k-eff, k-eff-COLD, was evaluated assuming that both the fuel and the Be temperatures are 293 K.

The [k-eff-HOT – k-eff-COLD] values shown in Table 7-1 indicate that the reactivity worth of the control mechanisms necessary to compensate for the temperature effect is significantly higher in Be-moderated HALEU cores than in non-moderated HEU and HALEU+ cores. The impact of the magnitude of the temperature feedback on the start-up procedure to safely and rapidly increase the power from zero to full power should be investigated to identify the pros and cons.

Table 7-1. Effect of temperatures on k-eff.

Fuel Form	FA identifier	Fuel Enrichment	FA pitch (cm)	[k-eff-HOT – k-eff-COLD][a]
(U,Zr)C/G, 35 vol% carbide, 17.6 mol% U in carbide	FA-1	HEU	2.68	+0.001
		HALEU	4.98	–0.074
(U,Zr)C, 7.1 mol% U	FA-3a/b/c	HEU	2.68	+0.002
		HALEU	5.10	–0.066
(U,Zr,Nb)C, 10.5 mol% U	FA-3a/b/c	HEU	2.68	–0.012
		HALEU	5.84	–0.067
(U,Zr,Ta)C, 20.2 mol% U	FA-3a/b/c	HEU	2.68	–0.009
(U,Zr)C, 18.7 mol% U	FA-2	HEU	2.68	–0.003
CERCER UN/ZrC, KVF_{comp} = 0.084	FA-3a/b/c	HEU	2.68	+0.002
		HALEU	5.18	–0.065
CERMET UN/W, KVF_{comp} = 0.310	FA-2	HEU	2.68	–0.006
CERMET UN/Mo, KVF_{comp} = 0.265	FA-2	HEU	2.68	–0.005
UC pins. External Cooling	FA-4/UC	HEU	2.68	–0.002
U pins. External Cooling	FA-4/U	HEU	2.68	–0.004
UC pins. Internal Cooling	FA-5/UC	HEU	2.68	–0.005
U pins. Internal Cooling	FA-5/U	HEU	2.68	–0.003
(U,Zr)C, 39 mol% U	FA-3a/b/c	HALEU+	2.68	–0.007
UC pins. External Cooling	FA-4'/UC	HALEU+	2.68	–0.005

[a] statistical uncertainty = ±0.001

8. Effect of Water Ingress on k-eff

NTP cores should remain subcritical even if accidentally submerged in water. To evaluate the effect of water ingress on k-eff, neutronics calculations were performed by filling the coolant channels with pure water with a density of 1.00 g/cm^3.

The values presented in Table 8-1 indicate that HEU and HALEU cores with limited parasitic neutron absorption, and, consequently, relatively small U^{235} loading, (i.e., (U,Zr)C/G, (U,Zr)C, (U,Zr,Nb)C, and CERCER) see their k-eff increase significantly when submerged. Such large increases in k-eff cannot be controlled by control drums only. Additional reactivity control mechanisms are necessary such as cadmium

wires inserted in coolant channels during transportation and take-off and to be removed in orbit before starting the reactor. It is noteworthy that all the HALEU cores considered here are in this category that require additional reactivity control mechanisms.

On the other hand, HEU cores with significant parasitic neutron absorption, and consequently relatively large U^{235} loading, (i.e., (U,Zr)C with W25Re cladding, (U,Zr,Ta)C, CERMET, and pins) see their k-eff decrease when submerged. Consequently, control drums should be sufficient to control the reactivity of these cores; additional control mechanisms should not be necessary. Hence, there may be trade-offs between the desire to use HALEU and to minimize the U^{235} loadings and the desire to simplify the control systems.

Table 8-1. Effect of water ingress on k-eff.

Fuel Form	FA identifier	Fuel Enrichment	FA pitch (cm)	[k-eff-COLD-FLOOD − k-eff-COLD][a]
((U,Zr)C/G, 35 vol% carbide, 17.6 mol% U in carbide	FA-1	HEU	2.68	+0.278
		HALEU	4.98	+0.180
(U,Zr)C, 7.1 mol% U	FA-3a/b/c	HEU	2.68	+0.271
		HALEU	5.10	+0.177
(U,Zr,Nb)C, 10.5 mol% U	FA-3a/b/c	HEU	2.68	+0.195
		HALEU	5.84	+0.127
(U,Zr,Ta)C, 20.2 mol% U	FA-3a/b/c	HEU	2.68	−0.052
(U,Zr)C, 18.7 mol% U	FA-2	HEU	2.68	−0.019
CERCER UN/ZrC, KVF_{comp} = 0.084	FA-3a/b/c	HEU	2.68	+0.264
		HALEU	5.18	+0.164
CERMET UN/W, KVF_{comp} = 0.310	FA-2	HEU	2.68	−0.047
CERMET UN/Mo, KVF_{comp} = 0.265	FA-2	HEU	2.68	−0.034
UC pins. External Cooling	FA-4/UC	HEU	2.68	−0.044
U pins. External Cooling	FA-4/U	HEU	2.68	−0.068
UC pins. Internal Cooling	FA-5/UC	HEU	2.68	−0.063
U pins. Internal Cooling	FA-5/U	HEU	2.68	−0.086
(U,Zr)C, 39 mol% U	FA-3a/b/c	HALEU+	2.68	+0.157
UC pins. External Cooling	FA-4′/UC	HALEU+	2.68	−0.052

[a] statistical uncertainty = ±0.001

9. Thermal and Hydraulics Aspects

As mentioned previously, all cores generate 300 MW and contain 211 FAs. The H_2 inlet/outlet temperatures are 350/2700 K. Assuming a radial peaking factor of 1.2, the peak FA generates 1.7 MW. The assumed axial power distribution in the peak FA is shown on Fig. 9-1.

The ideal orificing H_2 mass flow corresponding to inlet/outlet temperatures of 350/2700 K in the peak FA is 0.0437 kg/s. With an outlet pressure of 6 MPa, the corresponding H_2 outlet velocity would be 650 m/s (i.e., Ma = 0.18) under nominal operating conditions. This outlet pressure is consistent with those obtained in previous engine studies (see, for example, [Poston, 2018], [Belair, 2013], [Fittje, 2006]). Lower pressures would increase the H_2 outlet velocity accordingly (H_2 thermophysical quantities are almost independent of pressure for the temperature and pressure range of interest here and, consequently, so are the H_2 mass flow and heat transfer coefficients). Furthermore, since all FAs have the same H_2 flow surface area (1.246 cm^2), they also have the same axial H_2 velocity profile.

All FAs operate at Reynold Number of $1\text{-}8\times10^4$ corresponding to high mixing turbulent flows. The axial-dependent H_2 heat transfer coefficients are estimated with the standard Reynolds-Nusselt approach (with $Nu = 0.021 \times Re^{0.8} \times Pr^{0.4} \times [T_b/T_w]^{0.5}$, where T_b and T_w are the bulk H_2 and wall temperatures, respectively) and using temperature-dependent H_2 thermophysical data from [McCarty, 1981]. The H_2 heat transfer

coefficients increase from about 1.5 W/cm²K to about 3.5 W/cm²K between the inlet and the outlet primarily because, as H_2 heats up, its thermal conductivity increases by a factor of about 7 (from 0.002 to 0.015 W/cm·K).

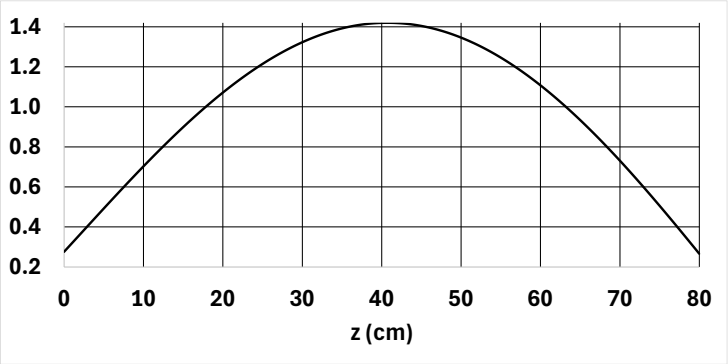

Fig. 9-1.
Axial power distribution
normalized to 1.

9.1 Block type FA

As a first approximation, a constant fuel thermal conductivity of 0.2 W/cmK was considered for the carbide solid solutions and for the composites (i.e., (U,Zr)C/G, CERMET and CERCER). Based on the data presented in section 2, this approach should yield conservative peak fuel temperature estimates. Note, however, that a perfect contact is assumed between the CERMETs and the W25Re cladding; this may be a non-conservative assumption unless, for example, a liquid metal bond such as tin is used. The fuel temperature gradients are estimated using the inverted fuel array approach presented in sections 2.7, 2.8, and 8.5.6 in [Todreas, 2021].

FA-1, FA-2, and FA-3a have the same H_2 flow surface area (1.246 cm²), H_2 velocity, heat transfer surface area (1925 cm²), and hydraulic diameter (0.207 cm). Consequently, the heat fluxes and heat transfer coefficients are also the same and so are the wall temperature axial profiles.

FA-3b and FA-3c have the same H_2 flow surface area and H_2 velocity as FA-1, FA-2, and FA-3a but they have larger heat transfer surface areas (2472 and 3019 cm², respectively), and smaller hydraulic diameter (0.161 and 0.132 cm, respectively) which yield lower wall temperatures.

For an H_2 outlet temperature of 2700 K, the estimated peak wall temperature is 2808 K for the 37-channel FAs (i.e., FA-1, FA-2, and FA-3a), 2765 K for FA-3b, and 2747 K for FA-3c. The estimated peak fuel temperature is 2942-3003 K for the 37-channel FAs, 2843 K for FA-3b, and 2785 K for FA-3c. For memory, the $(U_{0.071}Zr_{0.929})C$ and $(U_{0.39}Zr_{0.61})C$ melting temperatures are 3550 K and 3100 K, respectively.

Results are summarized in Table 9-1 and the axial temperature profiles are shown in Appendix D.

Table 9-1. Peak wall and peak fuel temperatures in FA-1, FA-2, and FA-3a/b/c assuming radial/axial peaking factors = 1.2/1.4.

	FA-1	FA-2	FA-3a	FA-3b	FA-3c
Peak H_2 outlet temperature (K)	2700	2700	2700	2700	2700
Peak wall temperature (K)	2808	2808	2808	2765	2747
Composite or carbide solid solution web thickness (cm)	0.244	0.209	0.256	0.199	0.163
Composite or carbide solid solution peak temperature (K)	2986	2942	3003	2843	2785
Composite or carbide solid solution peak power density (kW/cm³)	6.2	7.1	6.0	6.0	6.0
Composite or carbide solid solution peak ΔT at core midplane (K)[a]	303	238	328	199	133

[a] Temperature gradient between coolant channel walls and the middle of the web thickness.

An estimation of the peak ΔT_k (K) assuming 200-micron diameter kernels is also presented in Table 9-2. Despite large power densities (up to 120 kW/cm³ in the kernels) the ΔT_k are only a few Ks. Hence, from a temperature point of view, larger kernels may be acceptable. Other parameters such as the homogeneity of

the composite and the FA web thickness (1.6-2.6 mm, see Table 3-1) should also be considered to determine a preferred particle diameter.

Table 9-2. Peak power densities and ΔT_k in peak kernels assuming radial/axial peaking factors = 1.2/1.4.

	FA-1	FA-2	FA-3
Composite fuel type	(U,Zr)C/G	CERMET	CERCER
FA volume (cm^3)	498.3	498.3	498.3
Composite volume/FA (cm^3)	385.1	341.7	398.6
Fuel phase volume fraction in composite (KVF_{comp})	0.350	0.310[a] 0.265[b]	0.084[c] 0.050[d]
Peak composite power density (kW/cm^3)	6.20	6.99	5.99
Peak fuel phase power density (kW/cm^3)	17.7	22.5[a] 26.4[b]	71.3[c] 120[d]
Peak ΔT_k (K) in 200-micron diameter kernels	2[e]	2[a,f] 2[b,f]	5[c,f] 8[d,f]

[a] W/UN | [b] Mo/UN | [c] HEU | [d] HALEU | [e] Spherical carbide kernels are assumed though it is typically not the case, λ_k[(U,Zr)C] = 0.20 W/cmK | [f] λ_k[UN] = 0.25 W/cmK |

9.2 Pin type FA

The externally cooled pin type FA-4 and FA-4' have the same H_2 flow surface area (1.246 cm^2), H_2 velocity, heat transfer surface area (3779 cm^2), and hydraulic diameter (0.884 mm). Consequently, the heat fluxes and heat transfer coefficients are the also the same and so are the wall temperature axial profiles.

A perfect contact is assumed between the UC fuel and the W25Re cladding. This may be a non-conservative assumption unless, for example, there is a liquid metal bond such as tin. A perfect contact assumption is reasonable for liquid U.

For an H_2 outlet temperature of 2700 K, the estimated peak wall temperature for FA-4/UC and FA-4'/UC is 2737 K. The estimated peak fuel temperature for FA-4/UC and FA-4'/UC are 2740 and 2752 K, respectively. The estimated peak wall and fuel temperatures for FA-4/U are 2740 and 2757 K, respectively.

For the internally cooled pins of FA-5, the fuel temperature gradients are estimated with an inverted fuel array approach (see sections 2.7, 2.8, and 8.5.6 in [Todreas, 2021]). FA-5 has the same H_2 flow surface area and H_2 velocity as the externally cooled FA-4 and FA-4'. Its heat transfer surface area (3737 cm^2) is slightly smaller, and its hydraulic diameter (1.07 mm) is slightly larger than those of FA-4 and FA-4'.

For an H_2 outlet temperature of 2700 K, the estimated FA-5/UC peak wall and UC temperatures are 2739 and 2743 K, respectively. The estimated FA-5/U peak wall and U temperatures are 2741 and 2762 K, respectively.

Results are summarized in Table 9-3 and the axial temperature profiles are shown in Appendix E.

Table 9-3. Peak wall (W25Re) and peak fuel temperatures in FA-4, FA-4', and FA-5.

	FA-4/UC	FA-4'/UC	FA-4/U	FA-5/UC	FA-5/U
Peak H_2 outlet temperature (K)	2700	2700	2700	2700	2700
Peak wall (W25Re) temperature (K)[a]	2737	2737	2740	2739	2741
Peak fuel temperature (K)	2740	2752	2757	2743	2762
Peak fuel power density (kW/cm^3)	30.2	7.7	32.3	26.2	26.3
Peak ΔT fuel at core midplane (K)	27	185	79	46	92

[a] T_{melt}(W25Re) = 3500 K

10. Conclusion

A comparison of 300 MW NTP cores all containing 211 FAs but different fuel forms was presented.

Typical NTP fuel forms such as carbide solid solutions ((U,Zr)C and (U,Zr,X)C with X = Nb and Ta), carbide-graphite composites ((U,Zr)C/G), CERMETs (W/UN and Mo/UN), CERCERs (ZrC/UN), and carbonitride solid solutions ((U,Zr)CN) were considered. These typical NTP fuel forms are all manufactured as blocks with coolant channels.

In addition, two less typical NTP fuel forms were also considered: UC and U metal. These are manufactured as W25Re-clad pins.

HEU fuels (93% enriched U) that do not require additional in-core moderation were considered as well as HALEU fuels (19.75% enriched U) that require additional in-core moderation. Be was used for the in-core moderator.

For the HEU cores, the smallest U^{235} critical mass is obtained with the (U,Zr)C/G composite (62.3 kg) and the largest with the U metal pins (292 kg). The smallest BOM is obtained with the (U,Zr)C/G composite (930 kg) and the largest with the UN/W CERMET (2047 kg).

HALEU core BOMs are about twice as large as those of their HEU counterparts: 1854 vs 930 kg for the (U,Zr)C/G composite, 2187 vs 1172 kg for the CERCER and the (U,Zr)CN, 2153 vs 1167 kg for the (U,Zr)C, and 2562 vs 1223 kg for the (U,Zr,Nb)C. (As a reminder, these comparisons are meant to demonstrate trends and should not be understood as being comparisons between optimized fuel/core configurations.)

The required HALEU loading is very sensitive to the amount of in-core Be. Such large sensitivities translate into tight fabrication tolerances.

Temperature reactivity feedback is significantly higher in HALEU cores than HEU cores. The impact of the magnitude of the temperature feedback on start-up procedures to safely and rapidly increase the power from zero to full power should be investigated.

The HEU and HALEU cores with the smallest U^{235} loadings (i.e., (U,Zr)C/G, (U,Zr)C, (U,Zr,Nb)C, and CERCER) see their k-eff increase significantly if accidentally submerged and, consequently, require implementing control mechanisms in addition to control drums. All the HALEU cores considered here are in this category that require additional reactivity control mechanisms. The HEU cores with the largest U^{235} loadings (i.e., (U,Zr)C with W25Re cladding, (U,Zr,Ta)C, CERMET, and pins) see their k-eff decrease if accidentally submerged. Hence, there may be trade-offs between the desire to use HALEU and to minimize the U^{235} loadings and the desire to simplify the control systems.

It is to be noted that there are configurations with U enrichment slightly above HALEU (e.g., 25%) that may provide a compromise between the administrative preference for using HALEU and the engineering preference for simplifying the reactor systems as much as possible by, for example, not using in-core moderators.

11. References

Belair M., Sarmiento C., Lavelle T. (2013). Nuclear Thermal Rocket Simulation in NPSS, 49th AIAA-ASME-SAE-ASEE Joint Propulsion Conference.

Bhattacharyya S. K. (2001). An Assessment of Fuels for Nuclear Thermal Propulsion, ANL/TD/TM01-22.

Bobkov, V.P., Fokin, L.R., Petrov, E.E., Popov, V.V., Rumiantsev, V.N., Savvatimsky, A.I. (2008). Thermophysical Properties of Materials for Nuclear Engineering, IAEA-THPH, ISBN 978–92–0–106508–7.

Burkes D. E., Wachs D. M., Werner J. E., Howe S. D. (2007). An Overview of Current and Past W-UO2 CERMET Fuel Fabrication Technology, Proceedings of Space Nuclear Conference, Boston, MA.

Butt D. P., Wallace T. C. (1993). The U-Zr-C ternary phase diagram above 2473 K, J. Am. Ceram. Soc. 76 (6).

Cröll A., Williams J. K. P., Taylor B., Volz M. P., McKinney C., Coons T., Rosales J. (2025). Hot Hydrogen Testing of W-Coated UN Kernels in a Mo30W Matrix, Nuclear Science and Engineering, 199:1.

Das D., Dharwadkar S. R., Chandrasekharaiah M. S. (1981). Containment of Molten Uranium Alloys in Powder Metallurgical Tungsten Containers, Journal of Nuclear Materials 97.

Gustafson J. L. (2021). Space Nuclear Propulsion Fuel and Moderator Development Plan Conceptual Testing Reference Design. Nuclear Technology, 207(6).

Fittje J. E., Buehrle R. J. (2006). Conceptual Engine System Design for NERVA derived 66.7KN and 111.2KN Thrust Nuclear Thermal Rockets. AIP Conference Proceedings **813**, 502.

Fittje J. E., Borowski S. K., Schnitzler B. (2015). Revised Point of Departure Design Options for Nuclear Thermal Propulsion, AIAA SPACE 2015 Conference and Exposition.

Hamilton S. R., Zillinger J., Scott R., Jerred N., Palomares K., Salasin J., Miller V. M. (2024). Resilience of uranium mononitride/zirconium carbide composites and uranium-zirconium carbonitride in hot hydrogen for nuclear thermal propulsion. Journal of Nuclear Materials 596.

Hust J., Lankford A. (1984), Thermal conductivity of aluminum, copper, iron, and tungsten for temperatures from 1 K to the melting point. National Institute of Standards and Technology, Gaithersburg, MD.

Kardoulaki E. et al. (2022). Synthesis, thermal conductivity, and hydrogen compatibility of a high melting point solid solution uranium carbide, $(U_{0.2}Zr_{0.8})C$, Nuclear Materials and Energy 33.

Kardoulaki E. et al. (2025). Assessment of the hydrogen resistance of $(U_{0.2}Zr_{0.8})C$ following exposure up to 2327◦C, Ceramics International 51.

Knight T., Anghaie S. (1999). Processing Of Pseudo-Ternary Carbide Fuels For High Temperature Space Nuclear Reactors. Space Technology and Applications International Forum.

Kuznietz M., Livne Z., Cotler C., Erez G. (1988). Effect of Liquid Uranium on Tungsten Foils up to 1350 C. Journal of Nuclear Materials 160.

Lyon L. L. (1973). Performance of (U,Zr)C-Graphite (Composite) and of (U,Zr)C (Carbide) Fuel Elements in the Nuclear Furnace 1 Test Reactor, LA-5398-MS.

McCarty R. D., Hord J., Roder H. M. (1981). Selected Properties of Hydrogen (Engineering Design Data), National Bureau of Standards Monograph 168.

Nelson A. G., Kasam-Griffith A. A., Atz M. I. (2020). Performance of HALEU and HEU-Fueled Nuclear Thermal Propulsion Reactors, ANL/NSE-20/55.

Palomares K., Werner J. E. (2023). Assessment of Coated Particle Fuels for Space Nuclear Power and Propulsion Systems, NASA/CR−20230002635.

Pavlov T.R., Lestak M., Wenman M.R., Vlahovic L., Robba D., Cambriani A., Staicu D., Dahms E., Ernstberger M., Brown M., Bradford M.R., Konings R.J.M., Grimes R.W. (2020). Examining the thermal

properties of unirradiated nuclear grade graphite between 750 and 2500 K. Journal of Nuclear Materials 538.

Pelaccio D. G., El-Genk M. S. (1994). A review of nuclear thermal propulsion carbide fuel corrosion and key issues. Document ID 19950011802.

Peterson G. R., Carr R. E. Marinero E. E. (2023). Zirconium Carbide for Hypersonic Applications, Opportunities and Challenges. Materials 2023, 16, 6158.

Poston D. I. (2018). Design Comparison of Nuclear Thermal Rocket Concepts. ANS NETS 2018 – Nuclear and Emerging Technologies for Space.

Poston D. I. (2025). The Difficulties of Using a Neutron Moderator in Space Reactors. ANS NETS 2025 – Nuclear and Emerging Technologies for Space.

Raftery A. M., Seibert R. L., Brown D. R., Trammell M. P., Nelson A. T., Terrani K. A. (2021). Fabrication of UN-Mo CERMET Nuclear Fuel Using Advanced Manufacturing Techniques, Nuclear Technology, 207:6.

Schaeperkoetter J. et al. (2025). Impact of composition on the thermophysical properties of (U,Zr)C solid solution Carbide fuels. Journal of Nuclear Materials 607.

Schnitzler B, Borowski S. K., Fittje J. E. (2009). 25,000-lbf Thrust Engine Options Based on the Small Nuclear Rocket Engine Design. 45th AIAA/ASME/SAE/ASEE Joint Propulsion Conference & Exhibit.

Schnitzler B, Borowski S. K. (2010). Enrichment Zoning Options for the Small Nuclear Rocket Engine (SNRE). 46th AIAA/ASME/SAE/ASEE Joint Propulsion Conference & Exhibit.

Schnitzler B, Borowski S. K., Fittje J. E. (2011). Lower Thrust Engine Options Based on the Small Nuclear Rocket Engine Design. 47th AIAA/ASME/SAE/ASEE Joint Propulsion Conference & Exhibit.

Stewart M. E. M., Schnitzler B. G. (2013). A Comparison of Materials Issues for Cermet and Graphite- Based NTP Fuels, AIAA Annual Joint Propulsion Conference, San Jose, CA.

Tiwari J., Feng T. (2023). Intrinsic thermal conductivity of ZrC from low to ultrahigh temperatures: A critical revisit. Physical Review Materials **7**, 065001. DOI: 10.1103/PhysRevMaterials.7.065001

Todreas N. E., Kazimi M. S. (2021). Nuclear Systems Volume I: Thermal Hydraulic Fundamentals. Third edition. CRC Press.

Tucker S. D. (2019). CERMETS for Use in Nuclear Thermal Propulsion. Advances in Composite Materials Development. IntechOpen.

Vasudevamurthy G., Nelson A. T. (2022). Uranium carbide properties for advanced fuel modeling –A review, Journal of Nuclear Materials 558.

Wieselquist W. A., Lefebvre R. A. (2023). SCALE 6.3.1 User Manual, ORNL/TM-SCALE-6.3.

Youinou G. (2017). Preliminary Options Assessment of Versatile Irradiation Test Reactor: Neutron Fluxes in Test Reactors. INL/EXT-17-40962.

Youinou G., Lin C.S. (2022). Preliminary conceptual design of fast neutron spectrum nuclear thermal rocket cores using monolithic uranium nitride fuel, Progress in Nuclear Energy, 149.

Youinou G. Abou-Jaoude A. (2024). Preliminary Conceptual Design of Nuclear Thermal Rocket Reactor Cores Using Ceramic Fuels with Beryllium or Composite Neutron Moderators, Nuclear Science and Engineering, 198(8).

Appendix A: Estimation of Carbide Solid Solution Theoretical Densities With The Rule Of Mixtures

A.1 Binary Carbides

The molar mass M, molar volume V, and density ρ of a UC_x-ZrC_{1-x} solid solution can be obtained from those of UC and ZrC (Table A-1) as:

$M[UC_x\text{-}ZrC_{1-x}] = xM[UC] + (1-x)M[ZrC]$

$V[UC_x\text{-}ZrC_{1-x}] = xV[UC] + (1-x)V[ZrC]$

$\rho[UC_x\text{-}ZrC_{1-x}] = M[UC_x\text{-}ZrC_{1-x}] \div V[UC_x\text{-}ZrC_{1-x}]$

Table A-1. UC and ZrC molar mass M, molar volume V, and density ρ.

UC			ZrC		
M[UC] g/mol	ρ[UC] g/cc	V[UC] cc/mole	M[ZrC] g/mol	ρ[ZrC] g/cc	V[ZrC] cc/mole
249.4	13.63	18.30	103.2	6.73	15.33

The UC and ZrC volume fractions (z and (1-z), respectively) can be obtained as

$z = \{\rho[UC_x\text{-}ZrC_{1-x}] - \rho[ZrC]\} \div \{\rho[UC] - \rho[ZrC]\}$

The UC density in UC_x-ZrC_{1-x} is $z\rho[UC]$ and that of ZrC is $(1-z)\rho[ZrC]$.

The UC mass fraction is $z\rho[UC] \div \rho[UC_x\text{-}ZrC_{1-x}]$ and that of ZrC is $(1-z)\rho[ZrC] \div \rho[UC_x\text{-}ZrC_{1-x}]$.

Table A-2. Details of UC_x-ZrC_{1-x} theoretical density calculation as a function of the UC mole fraction (x).

UC mole fraction (x)	0.05	0.075	0.1	0.15	0.2	0.25	0.3
$V[UC_x\text{-}ZrC_{1-x}]$ cc/mole	15.48	15.56	15.63	15.78	15.93	16.08	16.22
$M[UC_x\text{-}ZrC_{1-x}]$ g/mol	110.5	114.2	117.8	125.1	132.4	139.8	147.1
$\rho[UC_x\text{-}ZrC_{1-x}]$ g/cc	7.138	7.339	7.538	7.930	8.315	8.694	9.065
UC volume fraction (z)	0.0591	0.0882	0.1171	0.1740	0.2298	0.2846	0.3384
gUC/cc in UC_x-ZrC_{1-x}	0.8054	1.2024	1.5956	2.3710	3.1319	3.8787	4.6120
UC weight fraction	0.1128	0.1638	0.2117	0.2990	0.3766	0.4462	0.5088
ZrC volume fraction (1-z)	0.9409	0.9118	0.8829	0.8260	0.7702	0.7154	0.6616
gZrC/cc in UC_x-ZrC_{1-x}	6.3323	6.1363	5.9421	5.5593	5.1836	4.8148	4.4528
ZrC weight fraction	0.8872	0.8362	0.7883	0.7010	0.6234	0.5538	0.4912

A.2 Ternary Carbides

The molar mass M, molar volume V, and density ρ of a UC_x-ZrC_y-XC_y solid solution with y = 0.5[1-x] can be obtained from those of UC, ZrC, and XC (Table A-3) as:

$M[UC_x\text{-}ZrC_y\text{-}XC_y] = xM[UC] + 0.5(1-x)M[ZrC\}] + 0.5(1-x)M[XC]$

$V[UC_x\text{-}ZrC_y\text{-}XC_y] = xV[UC] + 0.5(1-x)V[ZrC] + 0.5(1-x)V[XC]$

$\rho[UC_x\text{-}ZrC_y\text{-}XC_y] = M[UC_x\text{-}ZrC_y\text{-}XC_y] \div V[UC_x\text{-}ZrC_y\text{-}XC_y]$

Table A-3. NbC and TaC molar mass M, molar volume V, and density ρ.

X = NbC			X = TaC		
M[NbC] g/mol	ρ[NbC] g/cc	V[NbC] cc/mole	M[TaC] g/mol	ρ[TaC] g/cc	V[TaC] cc/mole
104.9	7.82	13.42	193.0	14.3	13.49

The UC, ZrC and XC volume fractions are z, u(1-z), and (1-u)(1-z) respectively with u = V[ZrC] ÷ {V[ZrC] + V[XC]}. When X = Nb, u = 0.5334. When X = Ta, u = 0.5319. Hence, the UC volume fractions z can be expressed as:

$z = \{\rho[UC_x\text{-}ZrC_{1-x}] - u\rho[ZrC] - (1-u)\rho[XC]\} \div \{\rho[UC] - u\rho[ZrC] - (1-u)\rho[XC]\}$

The UC density in $UC_x\text{-}ZrC_y\text{-}XC_y$ is $z\rho[UC]$, that of ZrC is $u(1-z)\rho[ZrC]$ and that of XC is $(1-u)(1-z)\rho[XC]$.

The UC mass fraction is $z\rho[UC] \div \rho[UC_x\text{-}ZrC_y\text{-}XC_y]$, that of ZrC is $u(1-z)\rho[ZrC] \div \rho[UC_x\text{-}ZrC_y\text{-}XC_y]$ and that XC is $(1-u)(1-z)\rho[XC] \div \rho[UC_x\text{-}ZrC_y\text{-}XC_y]$.

Table A-4. Details of $UC_x\text{-}ZrC_y\text{-}NbC_y$ theoretical density calculation as a function of UC mole fraction (x).

UC mole fraction (x)	0.05	0.075	0.1	0.15	0.2	0.25	0.3
$V[UC_x\text{-}ZrC_y\text{-}NbC_y]$ cc/mole	14.57	14.67	14.77	14.96	15.16	15.36	15.55
$M[UC_x\text{-}ZrC_y\text{-}NbC_y]$ g/mol	111.3	115.0	118.6	125.9	133.1	140.4	147.7
$\rho[UC_x\text{-}ZrC_y\text{-}NbC_y]$ g/cc	7.640	7.837	8.031	8.411	8.782	9.143	9.495
UC volume fraction (z)	0.0628	0.0936	0.1239	0.1834	0.2414	0.2979	0.3530
gUC/cc in $UC_x\text{-}ZrC_y\text{-}NbC_y$	0.8558	1.2751	1.6889	2.5001	3.2903	4.0604	4.8110
UC weight fraction	0.1120	0.1627	0.2103	0.2972	0.3747	0.4441	0.5067
ZrC volume fraction u(1-z)	0.4999	0.4835	0.4673	0.4355	0.4046	0.3745	0.3451
gZrC/cc in $UC_x\text{-}ZrC_y\text{-}NbC_y$	3.3641	3.2537	3.1447	2.9311	2.7230	2.5202	2.3225
ZrC weight fraction	0.4403	0.4152	0.3916	0.3485	0.3101	0.2756	0.2446
NbC volume fraction (1-u)(1-z)	0.4373	0.4230	0.4088	0.3811	0.3540	0.3276	0.3019
gNbC/cc in $UC_x\text{-}ZrC_y\text{-}NbC_y$	3.4201	3.3078	3.1970	2.9798	2.7683	2.5621	2.3611
NbC weight fraction	0.4477	0.4221	0.3981	0.3543	0.3152	0.2802	0.2487

Table A-5. Details of $UC_x\text{-}ZrC_y\text{-}TaC_y$ theoretical density calculation as a function of UC mole fraction (x).

UC mole fraction (x)	0.05	0.075	0.1	0.15	0.2	0.25	0.3
$V[UC_x\text{-}ZrC_y\text{-}TaC_y]$ cc/mole	14.61	14.71	14.80	15.00	15.19	15.38	15.58
$M[UC_x\text{-}ZrC_y\text{-}TaC_y]$ g/mol	153.1	155.7	158.2	163.3	168.3	173.4	178.5
$\rho[UC_x\text{-}ZrC_y\text{-}TaC_y]$ g/cc	10.48	10.59	10.69	10.89	11.08	11.27	11.46
UC volume fraction (z)	0.0626	0.0933	0.1236	0.1830	0.2409	0.2973	0.3524
gUC/cc in $UC_x\text{-}ZrC_y\text{-}TaC_y$	0.8537	1.2721	1.6849	2.4947	3.2837	4.0528	4.8027
UC weight fraction	0.0814	0.1202	0.1576	0.2291	0.2963	0.3596	0.4192
ZrC volume fraction u(1-z)	0.4986	0.4823	0.4662	0.4346	0.4038	0.3738	0.3445
gZrC/cc in $UC_x\text{-}ZrC_y\text{-}TaC_y$	3.3557	3.2458	3.1374	2.9247	2.7175	2.5155	2.3185
ZrC weight fraction	0.3201	0.3066	0.2935	0.2686	0.2452	0.2232	0.2024
TaC volume fraction (1-u)(1-z)	0.4387	0.4244	0.4102	0.3824	0.3553	0.3289	0.3031
gTaC/cc in $UC_x\text{-}ZrC_y\text{-}TaC_y$	6.2741	6.0686	5.8659	5.4682	5.0808	4.7031	4.3348
TaC weight fraction	0.5985	0.5732	0.5488	0.5022	0.4585	0.4173	0.3784

Appendix B: Estimation of Carbonitride Solid Solution Theoretical Densities With The Rule Of Mixtures

The approach is the same as that presented in Appendix A. Results are presented below.

Table B-1. UN and ZrC molar mass M, molar volume V, and density ρ.

UN			ZrC		
M[UN] g/mol	ρ[UN] g/cc	V[UN] cc/mole	M[ZrC] g/mol	ρ[ZrC] g/cc	V[ZrC] cc/mole
251.4	14.30	17.58	103.2	6.73	15.33

Table B-2. Details of UN_x-ZrC_{1-x} theoretical density calculation as a function of the UN mole fraction (x).

UN mole fraction (x)	0.05	0.075	0.1	0.15	0.2	0.25	0.3
V[UN_x-ZrC_{1-x}] cc/mole	15.45	15.50	15.56	15.67	15.78	15.90	16.01
M[UN_x-ZrC_{1-x}] g/mol	110.6	114.3	118.0	125.4	132.8	140.3	147.7
ρ[UN_x-ZrC_{1-x}] g/cc	7.161	7.374	7.585	8.004	8.416	8.823	9.224
UN volume fraction (z)	0.0569	0.0851	0.1130	0.1683	0.2228	0.2765	0.3295
gUN/cc in UN_x-ZrC_{1-x}	0.8138	1.216	1.616	2.406	3.186	3.954	4.711
UN weight fraction	0.1136	0.1649	0.2130	0.3007	0.3785	0.4481	0.5108
ZrC volume fraction (1-z)	0.9431	0.9149	0.8870	0.8317	0.7772	0.7235	0.6705
gZrC/cc in UN_x-ZrC_{1-x}	6.3470	6.1576	5.9695	5.5975	5.2307	4.8692	4.5127
ZrC weight fraction	0.8864	0.8351	0.7870	0.6993	0.6215	0.5519	0.4892

Appendix C: Neutron Spectra

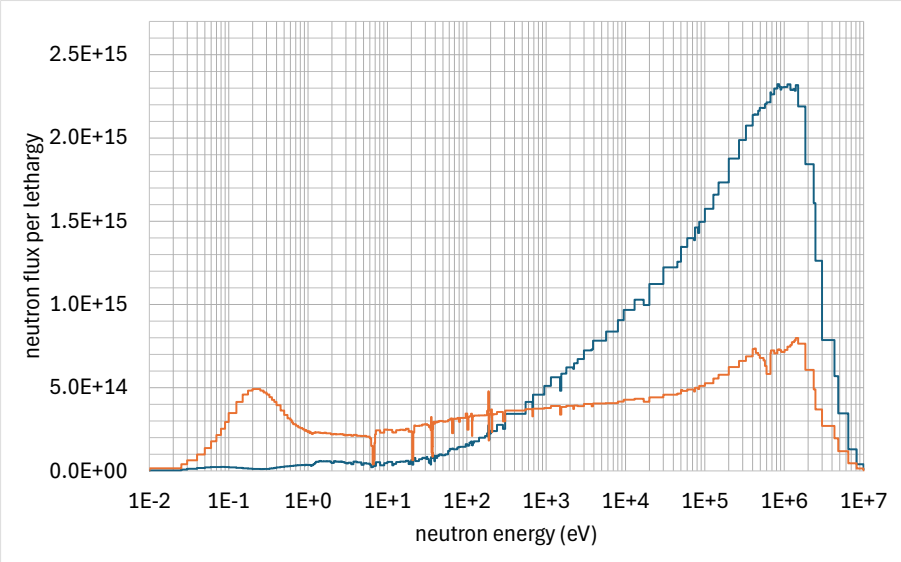

Fig. C-1.
Neutron spectra in HEU (blue) and Be-moderated HALEU (orange) (U,Zr)C/G composites with 17.6 mole% U in the carbide phase.

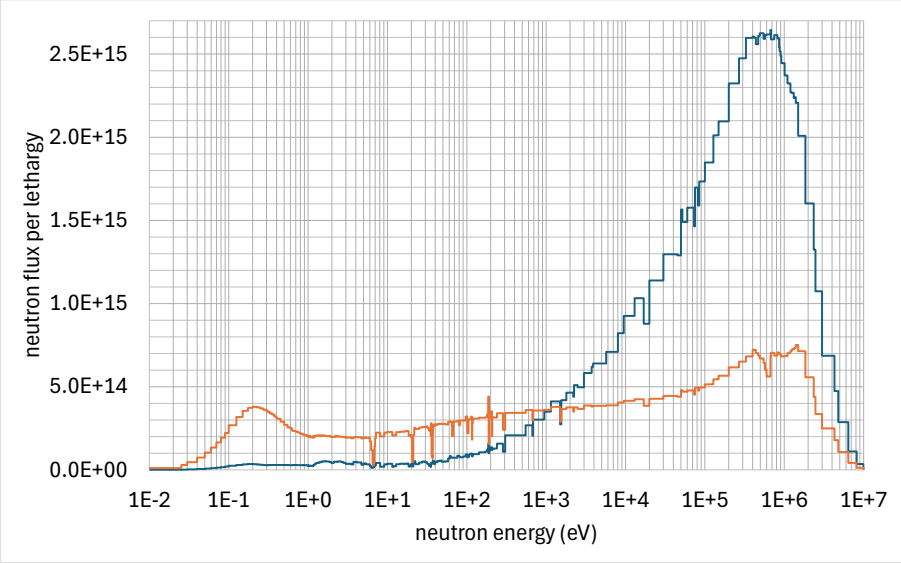

Fig. C-2.
Neutron spectra in HEU (blue) and Be-moderated HALEU (orange) (U,Zr)C solid solution with 7.1 mole% U.

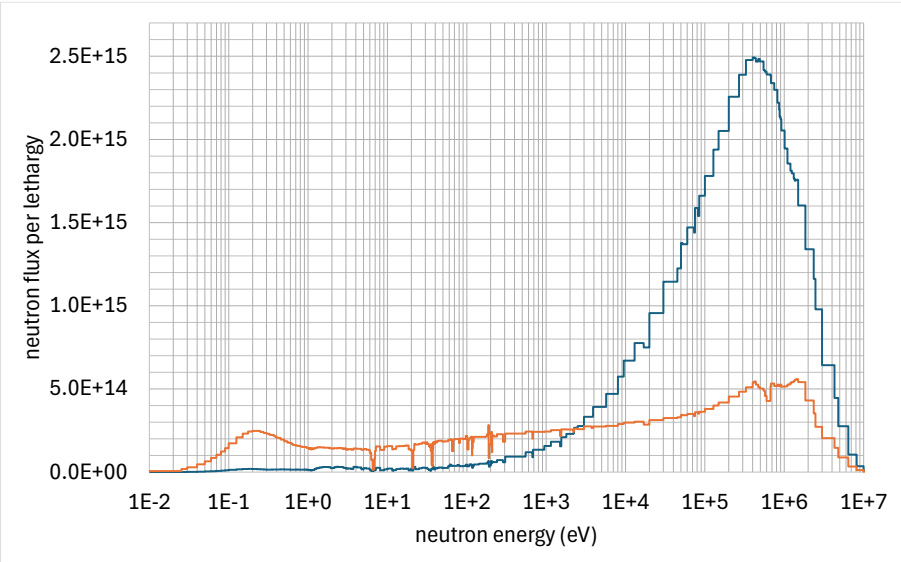

Fig. C-3.
Neutron spectra in HEU (blue) and Be-moderated HALEU (orange) (U,Zr,Nb)C solid solution with 10.5 mole% U.

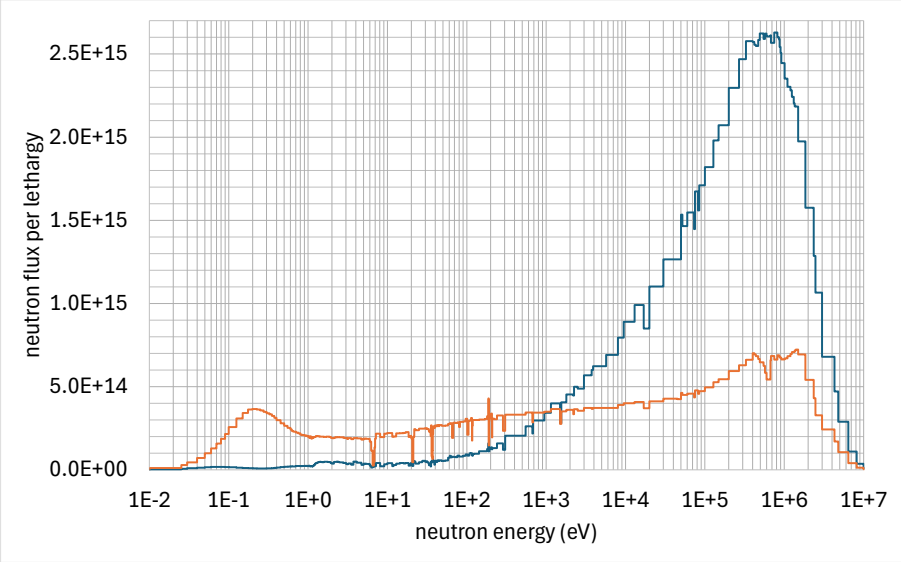

Fig. C-4.
Neutron spectra in HEU (blue) and Be-moderated HALEU (orange) UN/ZrC CERCER with 8.4 vol% UN.

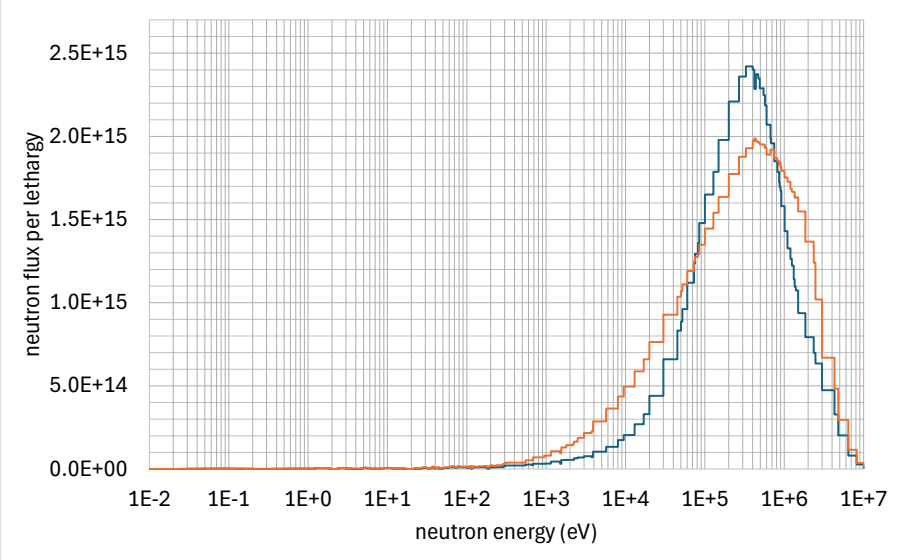

Fig. C-5.
Neutron spectra in HEU UN/W CERMET with 31 vol% UN (blue) and HEU UC/pins (orange).

Appendix D: Axial Temperature Profiles In The Peak FA-1, FA-2 And FA-3a/b/c

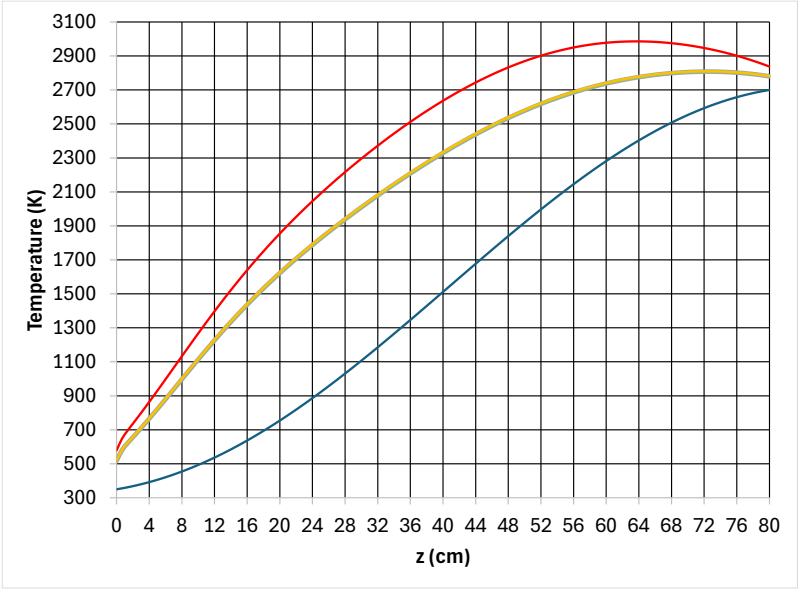

Fig. D-1.
H_2 bulk (blue), wall (yellow), and fuel centerline (red) axial temperature profiles in the peak FA-1 (37 coolant channels).

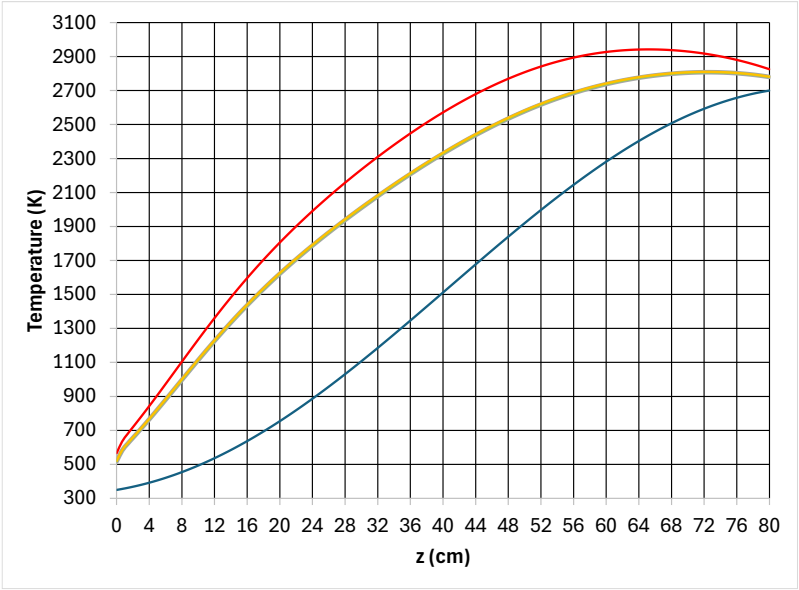

Fig. D-2.
H_2 bulk (blue), wall (yellow), and fuel centerline (red) axial temperature profiles in the peak FA-2 (37 coolant channels).

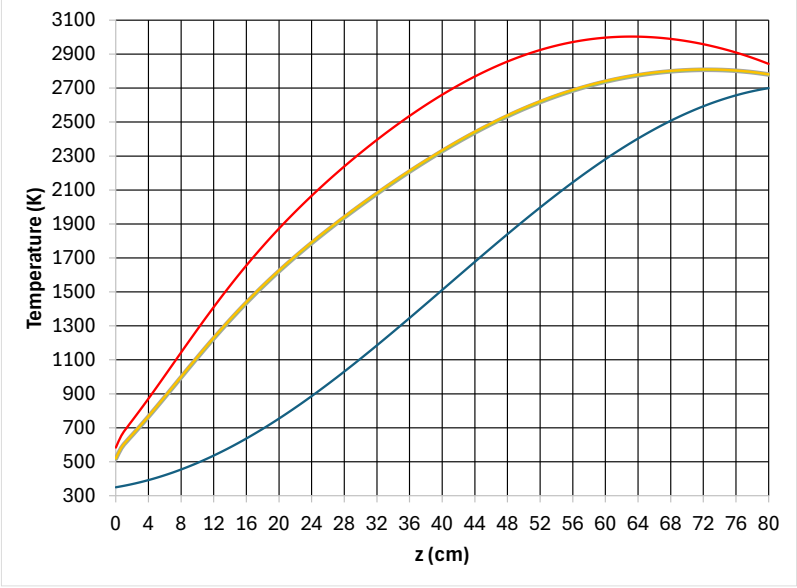

Fig. D-3.
H_2 bulk (blue), wall (yellow), and fuel centerline (red) axial temperature profiles in the peak FA-3a (37 coolant channels).

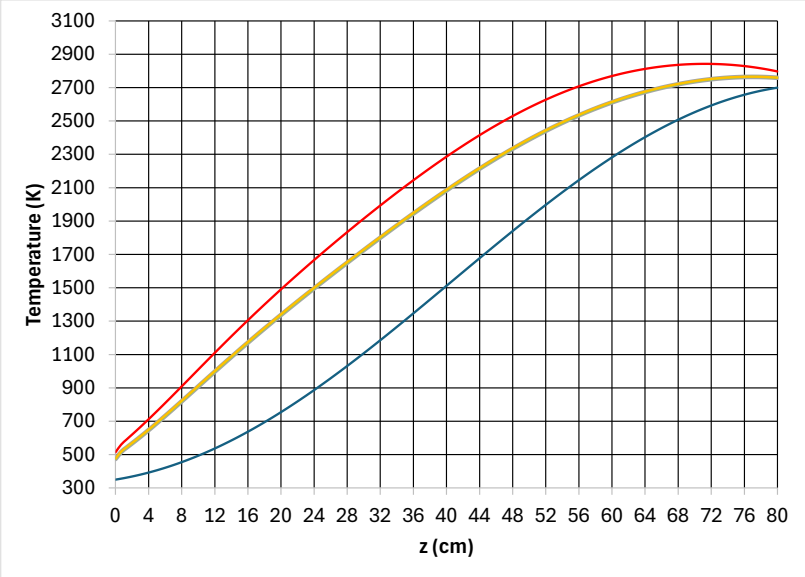

Fig. D-4.
H_2 bulk (blue), wall (yellow), and fuel centerline (red) axial temperature profiles in the peak FA-3b (61 coolant channels).

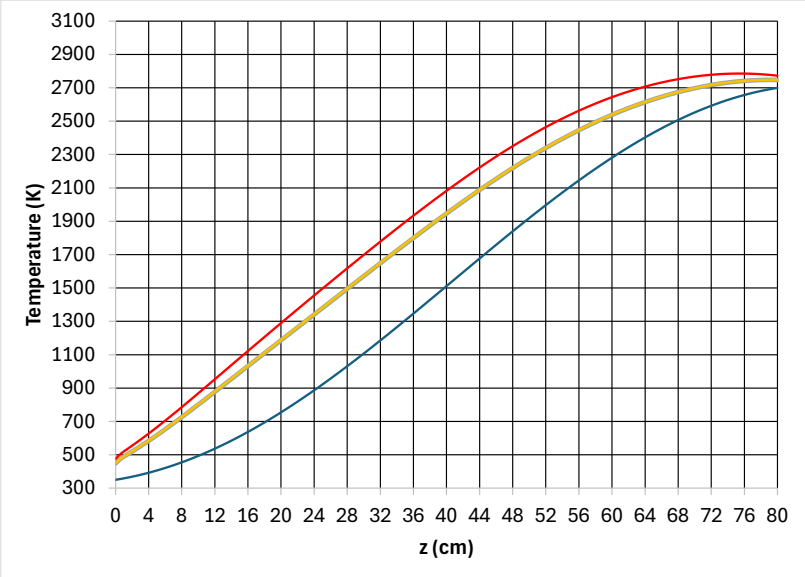

Fig. D-5.
H_2 bulk (blue), wall (yellow), and fuel centerline (red) axial temperature profiles in the peak FA-3c (91 coolant channels).

Appendix E: Axial Temperature Profiles In The Peak FA-4, FA-4′ And FA-5

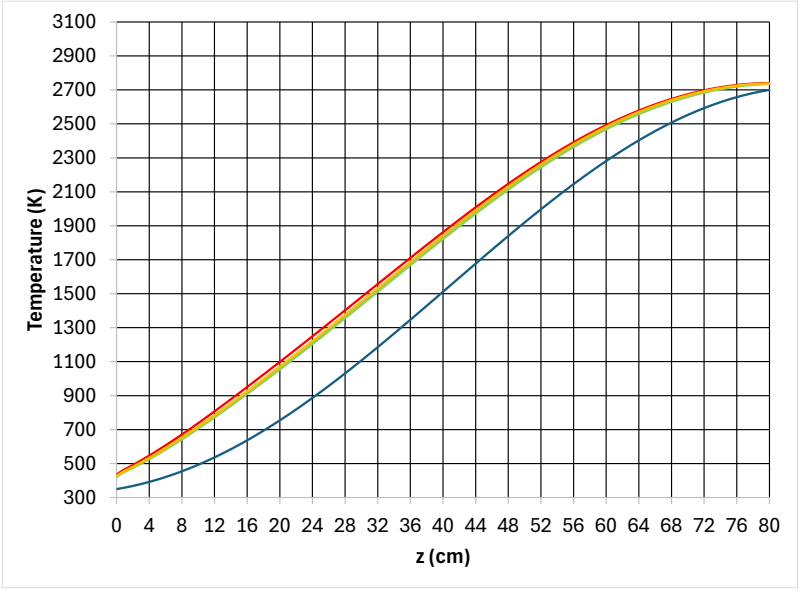

Fig. E-1.
H_2 bulk (blue), wall (yellow/green), and UC peak (red) axial temperature profiles in the peak FA-4/UC (externally cooled pins).

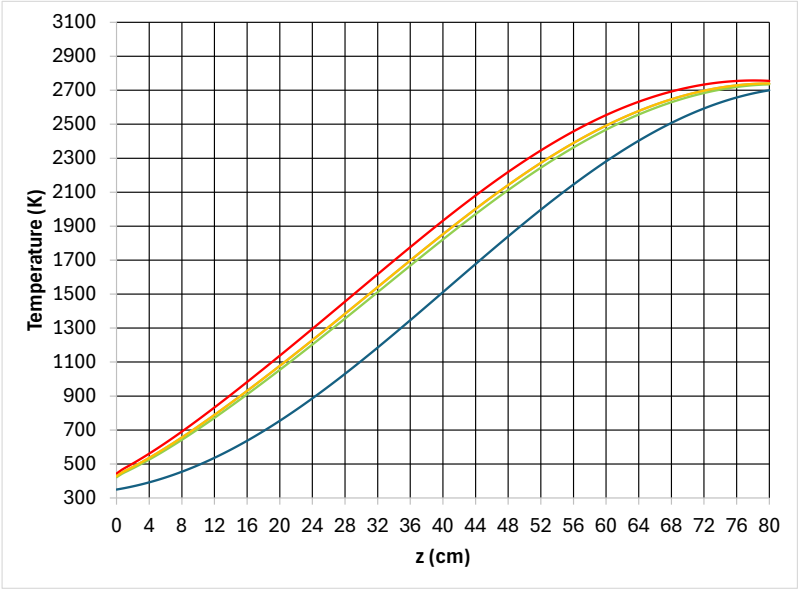

Fig. E-2.
H_2 bulk (blue), wall (yellow/green), and U peak (red) axial temperature profiles in the peak FA-4/U (externally cooled pins).

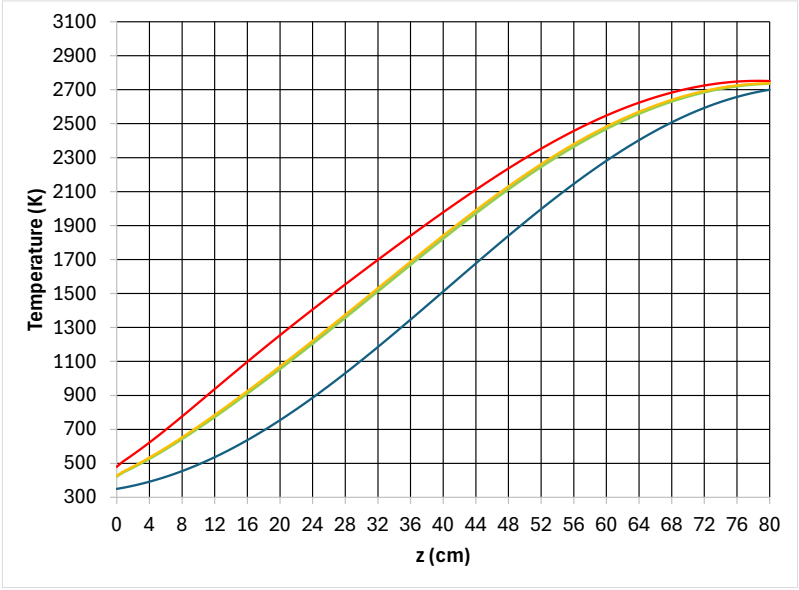

Fig. E-3.
H_2 bulk (blue), wall (yellow/green), and UC peak (red) axial temperature profiles in the peak FA-4′/UC (externally cooled pins).

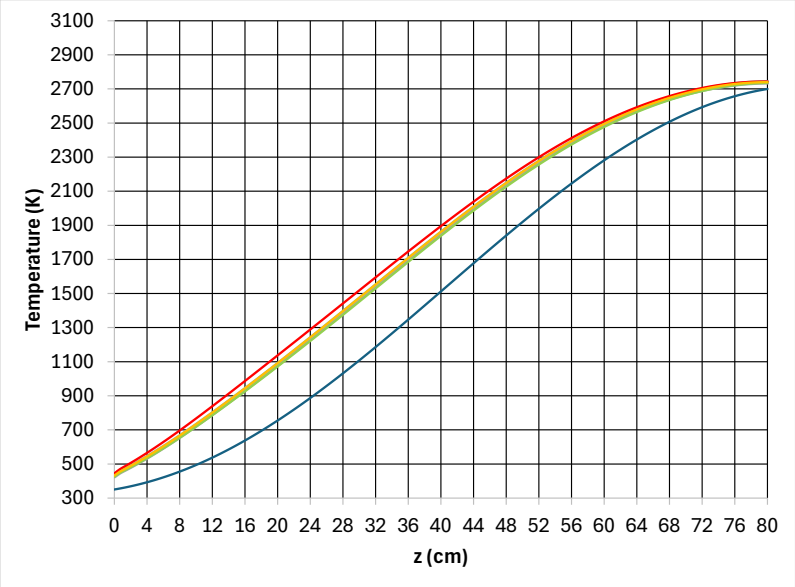

Fig. E-4.
H_2 bulk (blue), wall (yellow/green), and UC peak (red) axial temperature profile in the peak FA-5/UC (internally cooled pins).

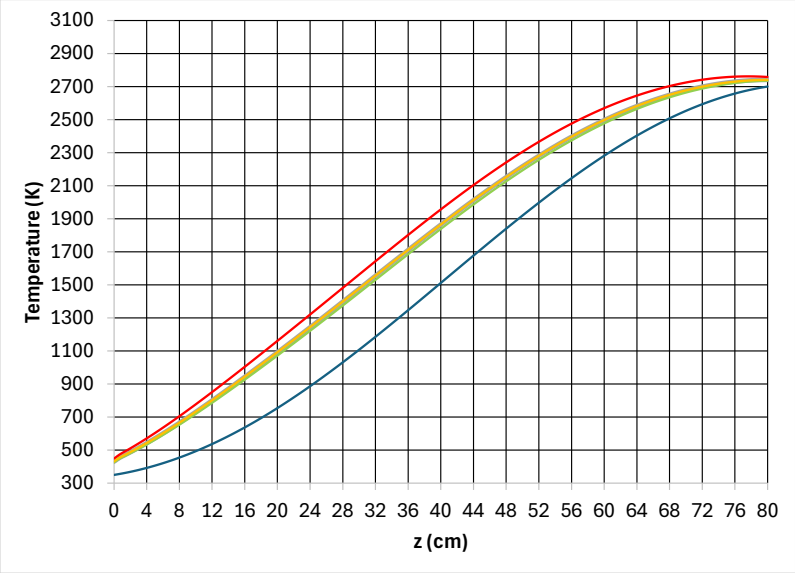

Fig. E-5.
H_2 bulk (blue), wall (yellow/green), and U peak (red) axial temperature profiles in the peak FA-5/U (internally cooled pins).